Karlsruhe Institute of Technology

Determination of the Synchrotron Radiation Pulse Length at the ANKA Storage Ring

Bestimmung der Synchrotronstrahlungspulslänge am ANKA-Speicherring

Diplomarbeit am
Laboratorium für Applikationen der Synchrotronstrahlung
Prof. Dr. Tilo Baumbach
Fakultät für Physik
Karlsruher Institut für Technologie

von

cand. phys.
Nicole Hiller

Hauptreferent:

Prof. Dr. Tilo Baumbach

Koreferent:

Prof. Dr. Günther Quast

Oktober 2009

Ich erkläre hiermit, dass ich die vorliegende Arbeit selbständig verfasst und keine anderen als die angegebenen Quellen und Hilfsmittel verwendet habe.

Karlsruhe, den 15. Oktober, 2009

Zusammenfassung

Während der letzten Jahre wurde aufgrund der großen Nachfrage eine Vielzahl neuer Elektronensynchrotrons gebaut die sich auf die Erzeugung von Synchrotronstrahlung spezialisiert haben. Synchrotronstrahlung zeichnet sich vor allem durch ihr kontinuierliches Spektrum aus, das vom fernen Infrarot bis hin zu harter Röntgenstrahlung reicht. Des Weiteren besitzt sie eine sehr hohe Brillanz und weist eine gepulste Intensitätsverteilung auf. Die Intensitätsverteilung der Strahlung spiegelt die Ladungsdichteverteilung der Elektronen im Synchrotron wieder. Ein kontinuierlicher Elektronenstrahl ist aufgrund der Tatsache, dass in Synchrotrons Radiofrequenz-Hohlraumresonatoren zum Einsatz kommen, nicht möglich. Es bilden sich Elektronenpakete, die als (Elektronen-)"Bunche" bezeichnet werden. Ihre Länge, die sogenannte "Bunchlänge", wird mit dem quadratischen Mittel (engl. root mean square) entlang der Bewegungsachse angegeben.
Die Bunchlänge und die Strahlenergie gehören zu den wichtigen Parametern einer Synchrotronstrahlungsquelle. Die Strahlenergie (kinetische Energie der Elektronen im Strahl) legt die Untergrenze der Wellenlänge der emittierten Strahlung fest. Je höher die Strahlenergie ist, desto weiter reicht das emittierte Spektrum in den Bereich kurzer Wellenlängen. Die Bunchlänge spiegelt sich in der Pulslänge der Synchrotronstrahlungspulse wieder.
Gerade für zeitaufgelöste Experimente ist es wichtig die Pulslänge genau zu kennen. Des Weiteren ist die Bunchlänge der Hauptparameter für die Erzeugung kohärenter Synchrotronstrahlung (CSR).

Inkohärente Synchrotronstrahlung wird generell emittiert. Für Wellenlängen die länger sind als die Bunchlänge kommt zusätzlich eine kohärente Emission hinzu. Die Kohärenz der Strahlung macht sich vor allem dadurch bemerkbar, dass die Intensität der Strahlung vom Quadrat der Teilchenzahl abhängt und nicht wie im inkohärenten Fall von der Teilchenzahl. Dies führt zu einer enorm gesteigerten Strahlungsleistung im langwelligen Bereich des Strahlungsspektrums.
Für die meisten Synchrotrons ist die Bunchlänge so lang, dass der Wellenlängenbereich in dem die emittierte Strahlung kohärent ist, bereits durch die Ausmaße des Strahlrohres so stark gedämpft wird, dass eine Nutzung der Strahlung nicht möglich ist. Es gibt jedoch weltweit ein paar Synchrotrons, die sich auf die Erzeugung kohärenter Synchrotronstrahlung im THz-Bereich (sub-millimeter Wellenlängenbereich) spezialisiert haben. Um dies zu erreichen muss die Bunchlänge drastisch reduziert werden, was durch die Wahl geeigneter Maschinenparameter und -einstellungen ermöglicht werden kann. Am Campus Nord des Karlsruher Instituts für Technologie (KIT), wo diese Arbeit entstanden ist, befindet sich eine solche Synchrotronstrahlungsquelle: ANKA (Ångströmquelle Karlsruhe).

Die Messung sehr kurzer Bunchlängen gestaltet sich als schwierig, da eine Messung idealerweise nicht invasiv sein sollte, also den Elektronenstrahl nicht beeinträchtigen sollte. Es besteht die Möglichkeit die Länge der Synchrotronstrahlungspulse zu messen, was jedoch aufgrund der kurzen Pulsdauern nur indirekt möglich ist.

In dieser Arbeit werden verschiedene Möglichkeiten diskutiert um die Pulslänge zu bestimmen. All diese Methoden werden am ANKA-Speicherring eingesetzt. Die Vor- und Nachteile der einzelnen Methoden werden erläutert und Verbesserungen, die an den bestehenden Aufbauten durchgeführt wurden, werden beschrieben.

Die erste Methode ist die Bestimmung der Bunchlänge aus der Messung der Frequenz der Synchrotronoszillation. Bei der Synchrotronoszillation handelt es sich um eine Schwingung der Elektronenpakete in longitudinaler Richtung (also entlang der Flugrichtung). Diese Schwingung ist proportional zur Bunchlänge. Die Messung gestaltet sich als unproblematisch und kann - nicht invasiv - während des Strahlbetriebes durchgeführt werden. Sie erfolgt über die Fourieranalyse des Signals einer “Stripline”. Bei einer “Stripline” handelt es sich um einen Detektor, der aus mehreren Metallstreifen besteht, die sich direkt im Strahlrohr befinden. Durch den vorbeifliegenden Elektronenstrahl wird in diesem Draht ein Signal induziert. Die Synchrotronfrequenz lässt sich im Frequenzspektrum des Signals finden.

Bei der zweiten Methode handelt es sich um die Bestimmung der Synchrotronstrahlungspulslänge im sichtbaren Wellenlängenbereich mit einer Streak Camera. Streak Cameras sind Geräte mit denen sich kurze Lichtpulse aufzeichnen lassen. Ihre Stärke liegt darin, dass sie es erlauben nicht nur die Pulslänge, sondern auch das komplette zeitliche Profil der Pulse aufzuzeichnen. Das Funktionsprinzip einer Streak Camera ist wie folgt: Ein einfallender Lichtpuls löst aus einer Photokathode Elektronen heraus, die die gleiche Intensitätsverteilung wie der einfallende Lichtstrahl aufweisen. Diese Photoelektronen werden dann auf einen Fluoreszenzschirm geleitet. Auf dem Weg dorthin durchlaufen sie ein sich schnell änderndes elektrisches Feld, das dafür sorgt, dass die zeitliche Verteilung der Elektronen in eine räumliche Verteilung auf dem Fluoreszenzschirm umgesetzt wird. Über einen Elektronenvervielfacher (“multi channel plate”) direkt vor dem Schirm wird das Signal zusätzlich verstärkt. Eine CCD-Kamera nimmt dann ein Bild des Fluoreszenzschirms auf. Da die Anzahl der erzeugten Photoelektronen von nur einem einzelnen Lichtpuls nicht genügt um eine Auswertung vorzunehmen, wird über einen längeren Zeitraum aufgezeichnet. Das führt dazu, dass das Signal von allen Lichtpulsen über mehrere Umläufe aufgezeichnet wird. Die Tatsache, dass nicht nur über mehrere Umläufe, sondern auch noch über eine Vielzahl von verschiedenen Pulsen (es befinden sich normalerweise etwa 100 Elektronenpakete im Speicherring) gemittelt wird, führt zur Beobachtung von länger-en Pulsen als erwartet. Verschiedene Verbesserungen des Aufbaus wurden durchgeführt: Zum einen wurde ein Bandpassfilter angeschafft, der die Auflösung verbesserte, da Dispersionseffekte im Detektor verringert wurden. Eine Mittelung über viele Aufnahmen, die den Effekt der Synchrotronoszillation berücksichtigt, verbessert die Auflösung weiter. Während der Durchführung dieser Arbeit wurde der ANKA-Speicherring mit einer neuen Elektronenquelle ausgestattet. Diese ermöglicht es nun den Ring nicht nur mit einer Vielzahl von Elek-

tronenpaketen zu befüllen, sondern auch mit nur einem einzelnen Bunch ("Singlebunch-Betrieb"). Die Verfügbarkeit dieses Betriebsmodus hat es schließlich erlaubt, dass eine eindeutige Zuordnung der Pulslänge zu dem zugehörigen Bunchstrom möglich war. Eine Zunahme der Pulslänge, die nicht über die Messung der Synchrotronfrequenz bestimmt werden kann und eine Deformation der Pulsform in Abhängigkeit vom Strahlstrom wurden beobachtet und analysiert. Sie stehen im Einklang mit Resultaten von Messungen an anderen Synchrotronstrahlungsquellen und numerischen Simulationen des Effekts.

Die dritte Methode, die in dieser Arbeit vorgestellt wird, ist die Ermittlung der Pulslänge aus dem Interferogramm von kohärenten THz-Strahlungspulsen. Für das Interfogramm wurde das Signal mit einem Bolometer (THz-Strahlungsdetektor) gemessen. Zuvor wird der einfallende Strahl mit einem Strahlteiler aufgeteilt und vor der Detektion werden die Teilstrahlen wieder vereinigt. Einer der Teilstrahlen wird auf seinem Weg in den Detektor jedoch einen etwas längeren oder kürzeren Weg als der andere zurücklegen. Die Verzögerung (engl. delay) ist modular. Das Signal wird in Abhängigkeit der Verzögerung gemessen. Die Pulslänge kann dadurch bestimmt werden, dass die Fouriertransformation des Interferogramms das Spektrum des Pulses liefert. Für kohärente Synchrotronstrahlung bestimmt die Pulslänge das Spektrum maßgeblich. Die Schwierigkeit dieser Messmethode liegt darin, die Einflüsse des Strahlteilers und das Untergrundsignal herauszurechnen, bzw. mit Vergleichsmessungen zu eliminieren. Die Resultate dieser Messung liefern einen durchweg kürzeren Wert für die Pulslänge als die anderen Messmethoden. Dies könnte daran liegen, dass nur ein Teil des Bunches kohärent emittiert und die Pulslänge für kohärente Strahlung damit kürzer ist als die für inkohärente Strahlung. Das genaue Verständnis der kohärenten Emission ist Teil der Forschungsarbeiten der THz-Gruppe.

Der Hauptteil dieser Arbeit bestand darin, die Umsetzung einer weiteren Pulslängenmessmethode, der sogenannten Intensitätsautokorrelation zu untersuchen. Dafür mussten zunächst einige Messungen zur Charakterisierung der Strahlung an den Beamlines durchgeführt werden. Dazu gehörte es, die lineare Abhängigkeit der Intensität vom Strahlstrom zu überprüfen und die Intensität der Strahlung an den verschiedenen optischen Ports zu vergleichen. Dabei wurde herausgefunden, dass die lineare Abhängigkeit des Strahlstroms gegeben ist, soweit der Strahlorbit stabil bleibt. Desweiteren wurde festgestellt, dass die optische Leistung der Strahlung im verwendeten Wellenlängenbereich am optischen Port der sich zurzeit im Aufbau befindlichen IR2 Beamline um den Faktor 3.6 höher ist, als am optischen Port der IR1 Beamline.
Bei einer Intensitätsautokorrelation handelt es sich um eine Methode, die standardmäßig zur Bestimmung der Pulslänge sehr kurzer Laserpulse verwendet wird. In dieser Form wird die Methode jedoch bisher noch nicht zur Messung der Synchrotronstrahlungspulslänge verwendet. Der Aufbau ähnelt dem eines Michelson-Interferometers, jedoch ist es nicht nötig den verschiebbaren Spiegel mit einer solchen Präzison zu steuern, da keine Interferenzmuster aufgelöst werden sollen. Der entscheidende Unterschied besteht in der Wahl des Detektors: Für eine Intensitätsautokorrelation wird ein nichtlinearer Detektor benötigt, dessen Signal eine quadratische Intensitätsabhängigkeit aufweist. Für den hier präsentierten Aufbau wurden dafür Zwei-Photonen-Absorptionsprozesse (engl. two photon absorption processes) in Halbleitern verwendet. Bei einem solchen Zwei-Photonen-

Prozess werden zwei Photonen zur gleichen Zeit am gleichen Ort absorbiert und erzeugen somit über einen virtuellen Zwischenzustand ein Elektronen-Loch-Paar. Ist die Rate dieser Erzeugung hoch genug wird ein messbares Stromsignal erzeugt. Als Autokorrelationssignal bezeichnet man das Messsignal in Abhängigkeit von der Verzögerung. Aus dem Autokorrelationssignal kann die Pulslänge der eingehenden Pulse bestimmt werden, wenn deren Form bekannt ist. Da die Intensität der emittierten Synchrotronstrahlung im Messbereich der verwendeten Detektoren (etwa 800-1100 nm) deutlich schwächer ist als die Intensität, bei der diese Methode sonst verwendet wird, mussten gewisse Verbesserungen am Aufbau vorgenommen werden um die Empfindlichkeit zu erhöhen. Das Ziel war, mit einer Intensitätsautokorrelation eine weitere kostengünstige, unabhängige Messung der Pulslänge aufzubauen. Im Rahmen dieser Untersuchung wurden mehrere Experimente mit einem gepulsten Laser durchgeführt um die Methodik des Aufbaus zu verstehen und Verbesserungen an der Messempfindlichkeit zu überprüfen. Des Weiteren wurden die Charakteristiken verschiedener Halbleiterdetektoren (LEDs und Photodioden) untersucht. Die Empfindlichkeit des Messaufbaus wurde drastisch erhöht, sodass schließlich selbst mit sehr niedrigen optischen Leistungen (etwa 150 μW) noch Messungen möglich waren.
Gleichzeitig wurde die Rate des Signals zum Untergrund dadurch enorm gesteiegert, dass für die Signalverstärkung der verzögerte Strahl und der unverzögerte Strahl mit unterschiedlichen Frequenzen “gechoppt” wurden und das vorverstärkte Signal mit einem Lock-In Amplifier zusätzlich gefiltert und verstärkt wurde. Die Systematik des Aufbaus wurde untersucht. Aus der experimentell erhaltenen unteren Auflösungsgrenze des Messaufbaus wurden Abschätzungen gemacht, wie hoch die optische Leistung des Synchrotronlichts sein müsste um ähnliche Messergebnisse zu erhalten. Dabei kam heraus, dass die Intensität des Synchrotronlichts um den Faktor zwei zu gering ist. Die Empfindlichkeit der eingesetzten Detektoren reichte knapp nicht aus um eine Bestimmung der Pulslänge der Synchrotronstrahlung zu erlauben. Unter Verwendung eines empfindlicheren Detektors, wie z.B. eines Photomultipliers (PMT), könnte eine weitere Verbesserung der Empfindlichkeit erzielt werden, allerdings müsste dafür der Aufbau abgeändert werden um auf die Geometrie eines solchen Detektors angepasst zu werden.

Contents

1. Introduction

Over the past years many electron synchrotrons dedicated to the production of synchrotron radiation, so called light sources, have been constructed to cater for the high demand of the rapidly growing user community. The main characteristics of synchrotron radiation are its wide, continuous spectrum ranging from the far infrared to the hard X-rays, its high brilliance, and its pulsed time profile. Because synchrotrons are powered by radio frequency cavities the electron beam cannot be continuous but exhibits a pulsed structure. In most practical cases the shape of these electron bunches can be approximated by a Gaussian. Their RMS (root mean square) length is referred to as the bunch length.
The bunch length along with the beam energy are important parameters of every synchrotron light source. The beam energy determines how short the wavelength of the emitted synchrotron radiation can be. The bunch length determines the length of the synchrotron radiation pulses, which is responsible for the resolution that can be achieved with time resolved measurements. The bunch length is also the main parameter for the creation of coherent synchrotron radiation (CSR).
In addition to the incoherent synchrotron radiation which is emitted over a wide spectrum, there is also a coherent emission of synchrotron radiation. This coherent emission can only occur for wavelengths which are longer than the bunch length. For most synchrotrons the bunch length is larger than a centimetre and the beam pipe is only a few centimetres in diameter, so coherent radiation is highly damped. However, there are a few machines in existence that specialise in the production of CSR in the THz-range (sub-millimetre wavelength), to fill the "THz-gap", because the creation of broadband coherent radiation in that wavelength range is challenging with other sources. One of these machines is the ANKA storage ring at the Karlsruhe Insitute of Technology (KIT) where this diploma thesis was written.
The intensity of incoherent THz-radiation is rather low, but for CSR the intensity is proportional not only to the number of particles in the bunch, but to its square, which leads to a great amplification in the photon flux, since a typical bunch contains between 10^8 and 10^{10} particles. Figure 1.1 illustrates the coherent and incoherent spectrum in more detail.
In order to produce CSR in the THz range, the bunch length needs to be compressed down

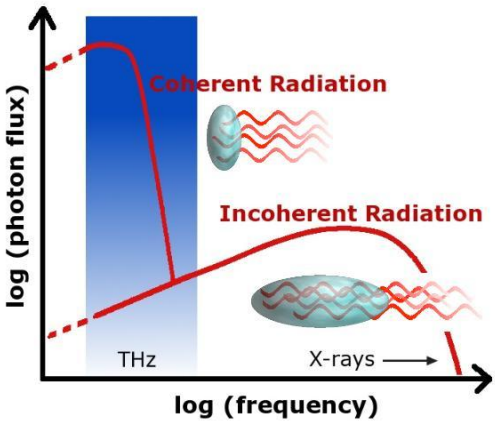

Figure 1.1: Sketch of the spectrum of the coherent and the incoherent synchrotron radiation for a fixed bunch length. The two bunches drawn in the picture illustrate that the emission of CSR is only possible for wavelengths with the size of the bunch length or larger, for shorter wavelengths the emission is incoherent.

to about a millimetre. This compression is achieved by gradually adjusting the accelerator optics. In order to monitor this compression process, the so called squeeze, in more detail, its key parameter - the bunch length - needs to be measured. The measurement of the bunch length should be non-invasive to the electron beam, which creates high demands on the resolution of the chosen method. Fortunately, the bunch length information is also imprinted into the emitted synchrotron radiation, so the compression of the bunches causes the synchrotron radiation pulses to be shorter as well. However, measuring pulse lengths in the picosecond range (1 ps $\cdot c \approx 0.3$ mm) brings along certain challenges as well [1] [2] [3].

The main objective of this work is to study the possibility of using a new type of measurement, the so called intensity autocorrelation, which is widely used to measure the length of short laser pulses, but has not yet been used with semiconductor detectors to measure the synchrotron pulse length [4]. The feasibility of this method and the experimental results have been studied.

In comparison to this independent measurement, the other methods which are used at the ANKA storage ring to determine the pulse length are introduced and their limitations are discussed. Furthermore, results obtained with the above mentioned methods in the framework of this thesis are presented.

The structure of this work is organised in the following way: In chapter 2 the basic concepts of accelerator physics are introduced in order to provide the reader with some background knowledge. The techniques currently used at the ANKA storage ring to determine the bunch length and the pulse length are explained in detail in chapter 3. An alternative method to determine the synchrotron pulse length - the intensity autocorrelation - is introduced in chapter 4 . The outcome of the autocorrelation measurements is presented and discussed in chapter 5. In chapter 6 measurements which have been carried out with a streak camera, one of the methods presented in chapter 3, are shown. A conclusion is given in chapter 7.

2. Concepts of Accelerator Physics

Today, particle accelerators are used in various fields of science, especially the generation and use of synchrotron radiation has opened up many applications in modern science. Synchrotron radiation is high on demand mainly because of its continuous spectrum ranging from the far infra-red to the hard x-rays and its high brilliance. Therefore a lot of synchrotron radiation sources, so called light sources, have been constructed over the past few years.

2.1 Particle Acceleration Using Alternating Fields

Modern particle accelerators reach particle energies of several GeV and even TeV, this however cannot be achieved with static electric fields, because of the necessary high field strengths. This problem was discovered soon after the development of particle accelerators using static electric fields in the early 20^{th} century, the answer, however, was brought up equally soon by Ising in 1925 [5], who suggested to use electric fields alternating at a high frequency, according to $V(t) = V_0 \sin(\omega t)$. The energy gain ΔE of a particle with charge q passing through such a field is:

$$\Delta E = qV_0 \sin \Psi_s \tag{2.1}$$

Ψ_s denotes a stable phase at which the particle travels through the field. With this concept, in theory, particles could be accelerated to any desired energy, given that they pass through a lot of these accelerating structures (linear accelerator) or many times through the same one (circular accelerator). The first linear accelerator (linac) using high frequency alternating fields was built in 1928 by Wideröe. Since then, alternating electric fields, usually referred to as RF fields (radio frequency fields), are being used in all modern accelerators for high particle energies.

Free electromagnetic waves do not have field components in the direction of propagation, therefore they are not suited for particle acceleration, however, when certain boundary

conditions are introduced in a way that plane electromagnetic waves exhibit longitudinal field components, they can be used for acceleration. In order to introduce such boundary conditions resonators are being used, the so called RF cavities in which a mode with a longitudinal electric field component is excited. A full derivation of the electric field can be found in [6], a sketch is given below. The Laplace equation for a field inside a cylindrical wave guide in cylindrical coordinates can be separated in a longitudinal and a transverse part, which can then be solved with Bessel functions. The solution represents many modes for which the boundary conditions are fulfilled. These modes can be divided into two main groups: the TE modes for which all the electric field components are transverse, and the TM modes which exhibit only transverse magnetic field components. The ones interesting for particle acceleration are the TM modes, because for these the electric field components are in the direction of propagation and the magnetic field components are not. TM modes are further characterised by three different indices TM_{npq}, here n is the azimuthal, p the radial, and q the longitudinal periodicity. For example, a TM_{010}-mode, which is used in RF cavities, has no longitudinal and azimuthal periodicity, but it has one node in radial direction at the wall, where the electric field must be zero. A rough sketch of the field pattern can be seen in Figure 2.1

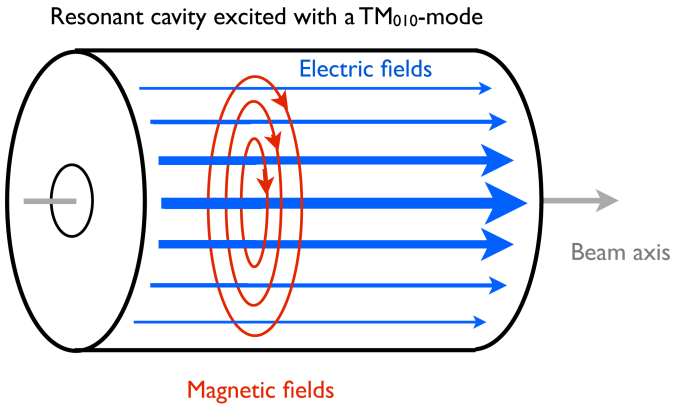

Figure 2.1: Schematic drawing of the field pattern inside a cylindrical resonant cavity excited with a TEM_{010}-mode. The electric field has only a longitudinal component whereas the magnetic field has no components along the beam axis.

The most commonly used accelerators today are the linac, the cyclotron and the synchrotron. Whereas cyclotrons can only be used for non-relativistic particle energies, they mainly play a role in the creation of radioisotopes and heavy ions for cancer treatments. In cyclotrons the fact that the revolution frequency of non relativistic-particles in a magnetic field is independent of the particle speed is used to guide the particles through an accelerating structure several times before they are extracted. A more detailed discussion of cyclotrons can be found in [6] [5].

The idea behind a linear accelerator is to assemble several RF cavities along a straight line with drift spaces in between to ensure that the particles always pass the RF cavities when they have the right phase.

Synchrotrons combine the ideas to have particles travel on a fixed "radius" and to use the same accelerating structure for many revolutions. To compensate the change in radius the energy gain brings along, the magnetic field used to keep the particles on their orbit has to be increased proportionally to the energy gain. A more detailed discussion of synchrotrons can be found in the following chapter.

2.2 Synchrotron

It was mentioned in the previous chapter, that in a synchrotron the particles are being kept on a constant orbit. In order to do so, the magnetic field strength in the bending magnets, which are used to keep the particles on that orbit has to be increased as the energy of the particles is increased during the acceleration process. The final energy which can be achieved with a synchrotron is limited by the strength of the bending magnets. However if the radius is chosen to be larger, then higher energies can be achieved, as less bending is required ($r \sim B^{-1}$). The size of synchrotrons in operation varies greatly, the smallest ones measuring only a few meters in circumference, and the largest one (LHC) having a circumference of nearly 27 km. Every synchrotron is built slightly different than the other ones, but the basic principles remain the same for all of them. Each is composed of the following components:

- An evacuated beam pipe
- An injection line
- RF cavities
- Magnets to shape and guide the beam

An evacuated beam pipe is required to achieve high particle energies, because otherwise they would be subjected to great losses due to interaction with air. The injection line is required to bring particles into the accelerator. The particles need to be already pre-accelerated because synchrotrons cannot operate over arbitrarily large energy scales. Various different types of RF cavities are used in different synchrotrons, some newer ones even being super-conducting. All these RF cavities have in common that they use the TM_{010}-mode, which was described in the previous chapter, to accelerate particles. There are several different types of magnets used in synchrotrons: The dipole or bending magnets are used to keep the particles on their nominal orbit. Quadrupole magnets are used to focus the beam, this is required because the particle beam stays within the synchrotron for various revolutions and, if left unfocussed, will quickly become intolerably large. A quadrupole magnet can only focus the beam in one direction and will defocus it in the other direction, but if two quadrupoles are placed after each other (with a drift space in between) and one of them focuses in the horizontal direction and the other one in the vertical direction then an overall focusing of the beam is achieved. The effects of the field inside a quadrupole are depicted in Figure 2.2. Due to the energy spread of the particles

this focusing will smear out, it can be compared to chromatic aberration in optics. Sextupole magnets are used to correct this chromaticity.

Synchrotrons can be used as storage rings to keep the particles circulating over many hours. There are ramping storage rings and storage rings with full energy injection.
In ramping storage rings the particles are injected at an energy that is lower than the desired operation energy, so the ring is filled during injection, while the field strength in the bending magnets is kept constant. Particles with the injection energy always pass the RF cavities at a phase at which they see a field that is large enough to restore the energy loss they undergo due to synchrotron radiation and other losses during every revolution. After the injection the energy is increased by slowly increasing the field strength of the bending magnets, then the particles arrive at the RF cavities at a slightly earlier time, thus causing them to see a higher field, which results in them gaining energy (a more detailed explanation of this effect can be found in chapter 2.4). To keep the particles inside the beam pipe, the magnetic field strength of the bending magnets has to be increased proportional to the growing particle energy. When the design energy is reached, the particles are being stored inside the synchrotron by just compensating their energy loss. Furthermore the beam current will decay slowly due to particles being lost completely for various reasons such as scattering with the rest gas. Once a certain limit is reached and only a fraction of the initial beam current is left, the remaining beam is dumped and a new injection is started after the machine is brought back to its injection settings.
For a full energy injection storage ring, the injected particles already have the desired energy and no further ramping is required, this has the advantage that the beam current can be kept rather constant, by injecting new particles into the storage ring frequently or even constantly.

2.3 Synchrotron Radiation

In 1947, the first visible synchrotron radiation was observed by Frank Elder, Anatole Gurewitsch, Robert Langmuir, and Herb Pollock at the General Electric synchrotron accelerator, hence the name. Beforehand there had already been predictions by Ivanenko and Pomeranchouk that the emission of electromagnetic radiation by the accelerated particles might limit the energies which could be reached by circular accelerators ([6] and references therein). Synchrotron radiation is generated when relativistic charged particles are deflected in a magnetic field. The produced radiation limits the maximum particle energy, because the particles emitting the radiation lose energy . As soon as more studies were undertaken and it was discovered that the synchrotron radiation had a very broad spectrum ranging from the far infrared to the hard X-rays and a very high brilliance, a lot of possible uses of this radiation opened up and special synchrotrons, so called synchrotron light sources were built, which are dedicated to produce more synchrotron radiation. The main characteristics of synchrotron radiation are presented in the following.

In a more general view radiation is emitted when charged particles are accelerated, however if the acceleration is parallel to the direction of propagation, as it is in linear accelerators,

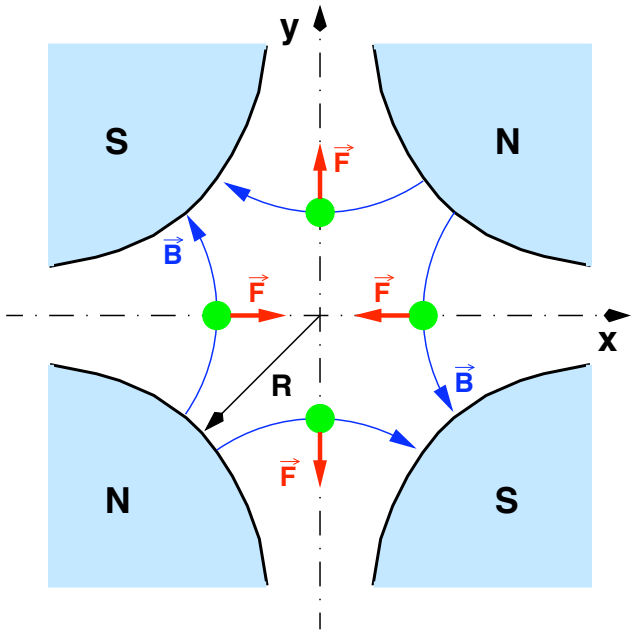

Figure 2.2: Schematic drawing of a horizontally focusing quadrupole. The positively charged beam travels along the z-axis. The blue lines show the direction of the magnetic field lines, the green dots mark particles passing the quadrupole at a certain position slightly away from the orbit on which they should be (right in the middle), the red arrows show in which direction the force acts onto the particles.

the power of the emitted radiation is independent of the particle energy and only depends on the energy increase per unit length, which results in a very low radiation power. For circular accelerators, however, the deflection of the particles is caused by an acceleration which is transverse to the direction of propagation and for this case the power of the radiation emitted by a single particle is:

$$P_s = \frac{e^2 c}{6\pi\epsilon_0 (m_0 c^2)^4} \frac{E^4}{R^2} \tag{2.2}$$

Where E is the particle Energy, R the radius of deflection and m_0 the rest mass of the particle. A full derivation of equation 2.2 can be found in [7]. From equation 2.2 it can already be seen that light-weight particles, such as electrons and positrons, emit a higher synchrotron radiation power than heavier ones. It is not surprising that all synchrotron light sources use electrons for this reason (positrons have the same radiation characteristics, but are more costly to produce). For electron synchrotrons, the total power emitted by the electron beam stored inside the ring is easily estimated with the following equation[7]:

$$P_\gamma = C_\gamma \frac{E^4(\mathrm{GeV}^4)}{\rho(m)} I_{\mathrm{beam}}(\mathrm{mA}) \tag{2.3}$$

Where Sands' definition of the radiation constant C_γ is used:

$$C_\gamma = \frac{4\pi}{3} \frac{r_c}{(m_e c^2)^3} = 8.8575 \cdot 10^{-5} m/GeV^3 \tag{2.4}$$

with r_c being the classical particle radius and m_e the rest mass of the electron. I_{beam} is the current of the electron beam stored inside the synchrotron. So the total optical power

of synchrotron radiation for a given particle energy is directly proportional to the beam current.

The angular distribution of the synchrotron radiation, emitted by an electron in its rest frame, is given by the following equation [8]:

$$\frac{P_s}{d\Omega} = \frac{e^2}{16\pi^2\epsilon_0 m_0^2 c^3}\left(\frac{d\vec{p}}{dt}\right)^2 \sin^2\Theta\,, \tag{2.5}$$

which is just the well-known equation for dipole radiation. When looking at this in the laboratory frame the toroid shape turns more and more into a cone, depending on the relativistic γ-factor ($\gamma = (1-\left(\frac{v}{c}\right)^2)^{-\frac{1}{2}} = \frac{E_{kin}+E_0}{E_0}$). The opening angle of the cone is inversely proportional to the γ-factor , as indicated in Fig 2.3.

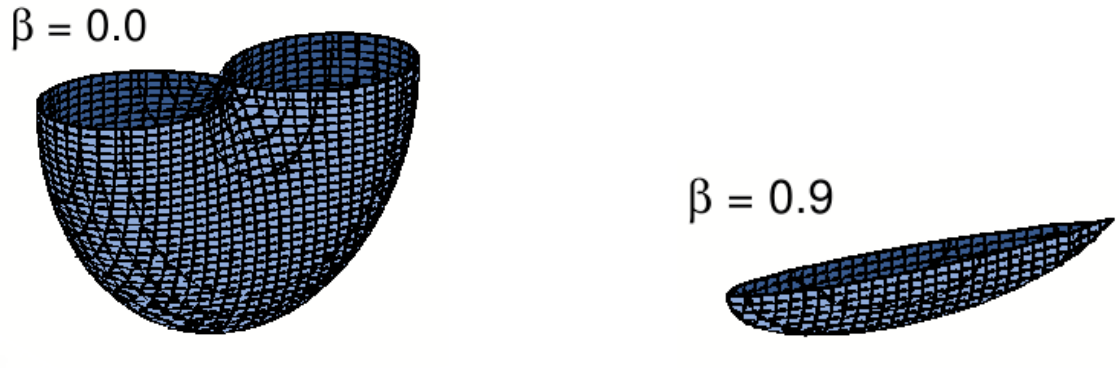

Figure 2.3: The shape of the angular distribution of synchrotron radiation. Left: For a particle at rest. Right: For a particle moving at $\beta = \frac{v}{c} = 0.9$

Because electrons are very light particles, highly relativistic energies are easily reached, so the opening angle of the cone in which the synchrotron radiation is emitted is very narrow, which allows easy extraction of the radiation through a beam pipe which is placed tangential to the bending radius. The radiation is then transported into a beamline where experiments are set up.

The spectrum of the synchrotron radiation and its dependence upon the beam energy is depicted in Figure 2.4. In the lower frequency region of the spectrum the power is hardly dependent on the energy, but in order to produce photons with a very high energy, a higher beam energy is required. The lower frequencies of the synchrotron radiation spectrum are mostly limited by the size of the beam pipe, because photons with a very low frequency cannot travel through a comparably narrow beam pipe. The energy E of a photon is $E = h\nu$ where ν is the photon frequency and h the Planck constant . The high frequency limit is slightly above the critical photon energy ϵ_c which divides the energy spectrum into two halves corresponding to equal emitted power. To calculate the critical photon energy for synchrotron radiation caused by electrons deflected inside bending magnets, an easy to use equation can be applied [6]:

$$\epsilon_c(\mathrm{keV}) = 0.665 \cdot E^2(\mathrm{GeV}^2) \cdot B(T) \tag{2.6}$$

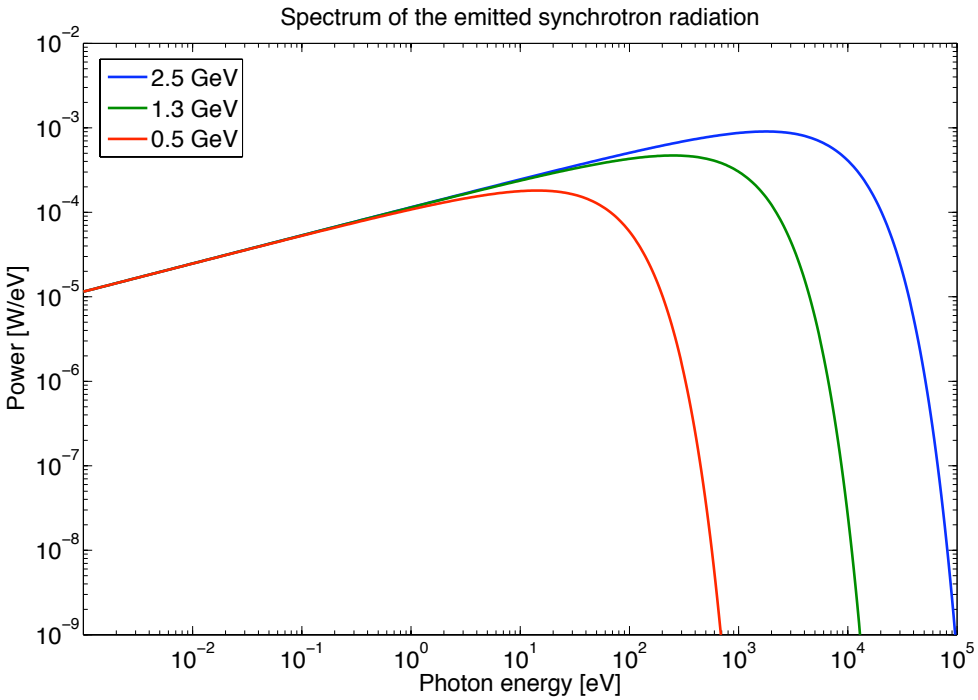

Figure 2.4: Spectrum of the emitted synchrotron radiation for different beam energies. The actual power was calculated with XOP [9] for the ANKA synchrotron radiation source.

2.4 Bunch Length

All particle accelerators using RF fields have one thing in common: They cannot form a continuous beam. This is because the electric field alternates and has the wrong polarity for acceleration for half the time of every period. This is why a bunched beam is created. The RF voltage itself causes a focusing of the beam in longitudinal direction, the so called phase focusing. Figure 2.5 depicts this. For relativistic particles in a synchrotron the orbit is slightly shorter when their momentum is smaller than the nominal momentum because they will be deflected more inside the bending magnets which results in them arriving at the RF cavity slightly earlier than the particles with the nominal momentum, vice versa, particles with a slightly higher momentum arrive a little later. For the acceleration the phase is such that the voltage seen by the beam lies between V_0 and 0, this has the advantage that the beam is automatically focused in longitudinal direction, because particles with a too low momentum will receive a higher energy gain than particles arriving at a slightly later phase. This effect is called phase focusing and results in the particles oscillating around the nominal phase Ψ_s.

The oscillation of the particles around the nominal phase Ψ_s with the frequency f_s is called the synchrotron oscillation. To make sure that particles always arrive with the correct phase after a revolution, the accelerator circumference needs to be designed to be an integer multiple of the RF wavelength. This integer multiple is then called the harmonic number h. The synchrotron tune Q_s is the synchrotron frequency f_s divided by the revolution frequency f_{rev} whereas $f_{rev} = \frac{f_{RF}}{h}$ with f_{RF} being the RF frequency.

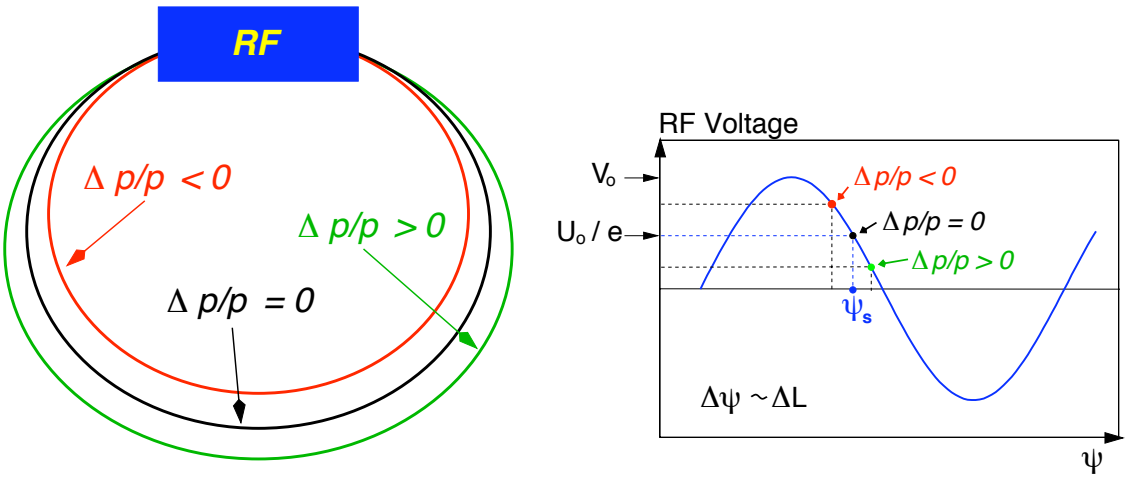

Figure 2.5: Particles with a momentum which is smaller than the nominal momentum travel on a slightly shorter orbit than particles with a higher momentum. Because the particles are relativistic, a shorter orbit will cause them to arrive at the RF-cavity at an earlier phase which will result in them being affected by a higher field. This means they will get a higher energy gain than particles with a too low momentum, who arrive later. This effect is called phase focusing.

The bunch length is an important parameter of a synchrotron light source, because it causes the synchrotron radiation observed at a beamline to exhibit the same time structure as the charge distribution of the electrons passing by. Therefore the length of the electron bunches is also approximately the length of the synchrotron radiation pulses. There is a slight elongation of the synchrotron pulse length because the electrons travel at a slightly lower velocity than the emitted photons. Consequently the observer at the beamline sees photons coming from a small angle and this causes the radiation pulse emitted by a single electron to have a finite duration. However, this finite duration δt, which is given by [7]:

$$\delta t = \frac{4\rho}{3c\gamma^3} \tag{2.7}$$

is very small for relativistic electrons, where γ is $> 10^3$ and ρ is the bending radius of the dipole magnet (several meters) which is causing the synchrotron radiation emission. So δt is in the order of several tens of attoseconds (10^{-17} s), whereas the typical bunch length of synchrotrons ranges from several hundred femtoseconds to several nanoseconds ($10^{-13} - 10^{-9}$ s). There is a large variety of different applications for synchrotron radiation, different pulse lengths are preferred for different experiments. Short pulse lengths are mainly interesting for time resolved measurements, like pump probe experiments. Short pulse lengths also play a great role for the creation of coherent synchrotron radiation which will be discussed in the next section (2.5).

The bunch length σ_z is defined as RMS (root mean square) value of any given particle distribution along the time axis (for a Gaussian pulse shape, this is the standard deviation), as depicted in Figure 2.6. For the pulse length of the synchrotron radiation pulses, it is common to use the FWHM (full width half maximum) instead.

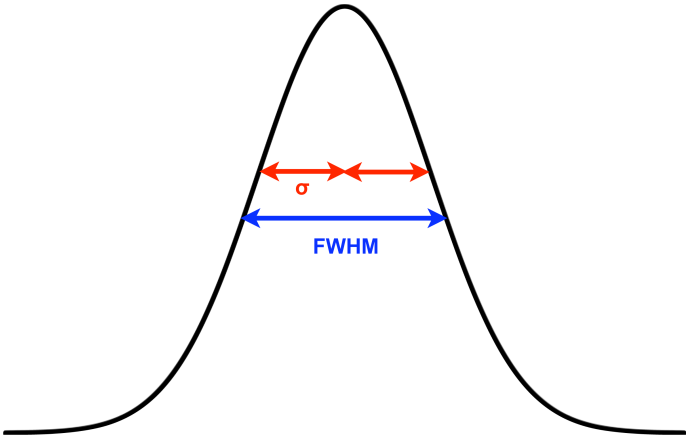

Figure 2.6: The relation between the standard deviation σ and the full width at half maximum (FWHM) for a Gaussian shaped pulse $\text{FWHM}_{Gaussian} = 2 \cdot \sqrt{2 \ln 2} \cdot \sigma \approx 2.35\sigma$

The bunch length for an infinitesimal current is given by [10]:

$$\sigma_z = \frac{c\sigma_\delta |\alpha_c - \gamma^{-2}|}{2\pi Q_s f_{rev}} \tag{2.8}$$

Here σ_δ is the RMS energy spread of the electrons which can be measured or calculated. α_c is the momentum compaction factor which gives the relation between the relative path length difference the particles obtain from a relative momentum difference:

$$\frac{\Delta L}{L_0} = \alpha_c \frac{\Delta p}{p_0} \tag{2.9}$$

Here L_0 is the length of the reference orbit on which a particle with reference momentum p_0 travels. A lower momentum compaction factor means that a particle with a too high momentum only travels along a slightly longer path.

A bunch lengthening with increasing single bunch current has been observed at several synchrotrons, which is most likely due to potential well deformations. The bunch length increases slightly with the bunch current for lower bunch currents [11] [12], but for higher bunch currents a steeper increase has been observed, since other effects influence the bunch length above a certain threshold current.

Another effect that occurs is a bunch deformation. If the bunch current is very high, the shape will not be Gaussian anymore but move towards a shape that is very steep in the front (head) and has a nearly slow decrease towards the end (tail) of the bunch [8]. If the bunches are shorter, then this effect occurs at lower bunch currents already. In the case of very short bunches, this is most likely caused by coherent synchrotron radiation wake-fields .

2.5 Coherent Synchrotron Radiation (CSR)

Because of the bunched structure discussed in chapter 2.4, the emission of synchrotron radiation is coherent for photon wavelengths which are equal to or longer than the bunch

length [7]. An illustration of the produced spectrum can be found in Figure 2.7. The power of this coherent radiation is not proportional to the beam current I_{beam} as in equation 2.3, but proportional to I^2_{beam} which leads to a great rise in power for these long wavelengths. Radiation with a wavelength that is in the order of the size of the diameter of the beam pipe or longer is significantly damped due to radiation shielding by the beam pipe itself, which is a fortunate effect, otherwise losses in synchrotrons would be significantly higher. The production of coherent synchrotron radiation with wavelengths in the infrared and THz-region (μm to mm) by shortening the bunch length has opened up new opportunities in various fields of research. Especially as the production of broadband coherent THz-radiation with lasers is rather tricky and does not yield the optical power produced by CSR. The shortening of the bunch length in synchrotrons can be achieved by changing the settings for the quadrupole and sextupole magnets in a way that the momentum compaction factor α_c, which was introduced in equation 2.9, is decreased. For CSR there is a so called bursting-stable threshold, if the bunch current is below this threshold, which increases with the bunch length, then the emission of the CSR is stable, but if the current is above that threshold the emission depicts a bursting behaviour [13].

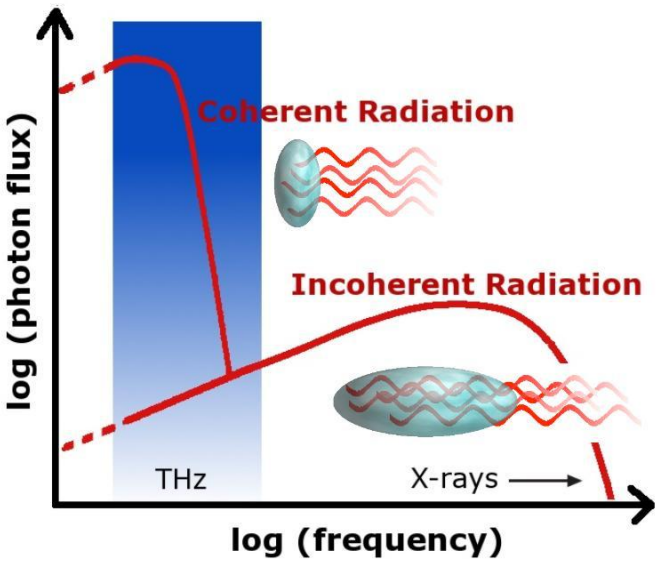

Figure 2.7: Sketch of the spectrum of the coherent and the incoherent synchrotron radiation for a fixed bunch length. The two bunches drawn in the picture illustrate that the emission of CSR is only possible for wavelengths with the size of the bunch length or larger, for shorter wavelengths the emission is incoherent.

2.6 ANKA - Ångström-Source Karlsruhe

The synchrotron radiation source ANKA is located at the campus north of the Karlsruhe Institute of Technology. The first beam was seen in 2000 and since 2003 it has taken up operation for users. 12 beamlines are currently being used with 4 new ones being built at the moment.

The drawing of the ANKA facility in Figure 2.9 illustrates the chain of pre-accelerators: First the electron beam is created by the electron gun, where it is accelerated to 90 keV,

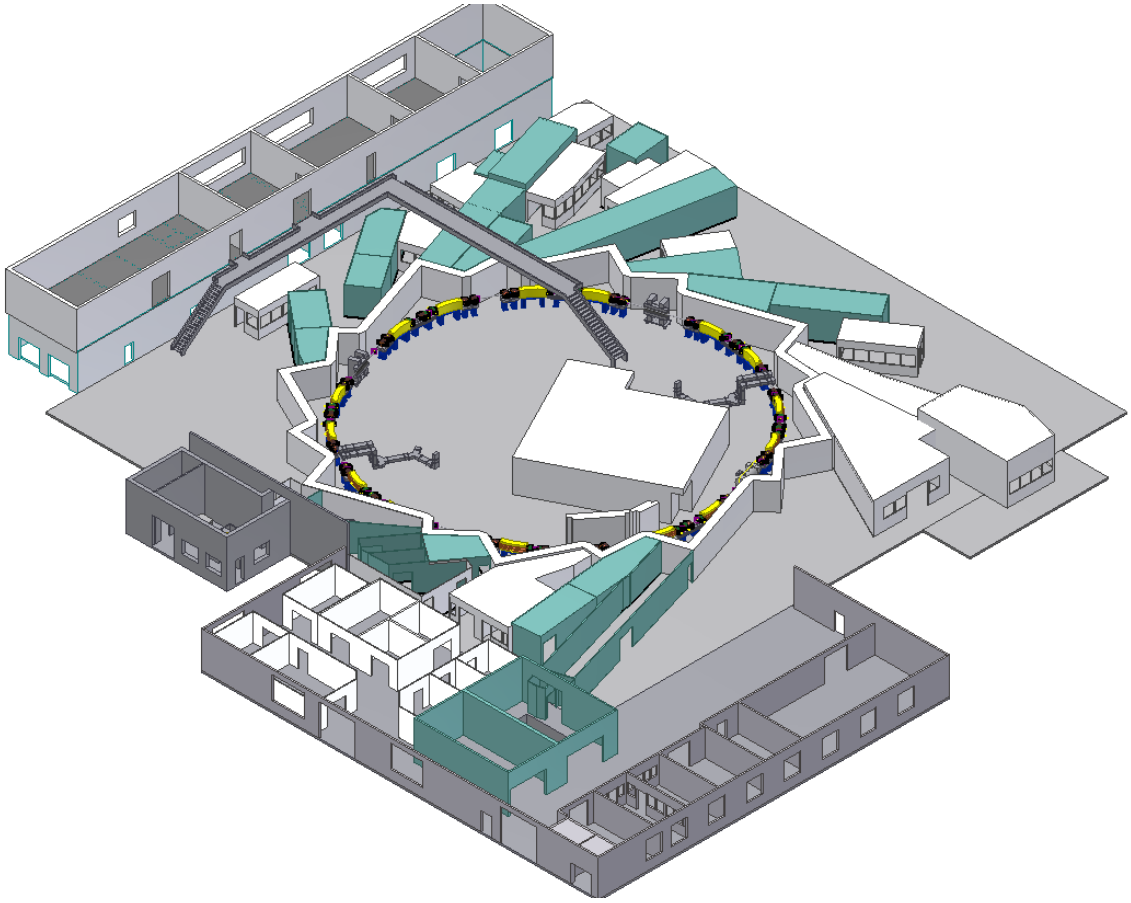

Figure 2.8: Drawing of the ANKA facility at the campus north of the Karlsruhe Institute of Technology. The ring is only shielded by a 3 m high concrete wall which is built around it.

then it passes a microtron where the particle energy is further increased to 53 MeV. The beam is then directed into the booster synchrotron where the electrons are accelerated to 500 MeV, at this energy they are injected into the storage ring. In the storage ring the energy can then be increased up to 2.5 GeV.

ANKA has two main operation modes for users. The standard one is the normal user operation. About one day a month there is a special user operation mode, the so called "low-α_c-operation" during which the momentum compaction factor α_c is decreased by changing the settings of the quadrupole and sextupole magnets, so shorter bunch lengths are achieved which leads to the creation of CSR. The parameters for the different operation modes have been summed up in Table 2.6. In addition to the normal user operation and the special user operation, there are machine physics days during which accelerator studies with beam are performed. At the moment, during user operation there is always a multi-bunch filling pattern created, this means that the charge distribution inside the ring exhibits many bunches over one revolution. The standard for ANKA is a filling pattern with 99 bunches grouped into three trains, this is depicted in Figure 2.10. This filling pattern is chosen for the standard operation because it allows a high amount of current

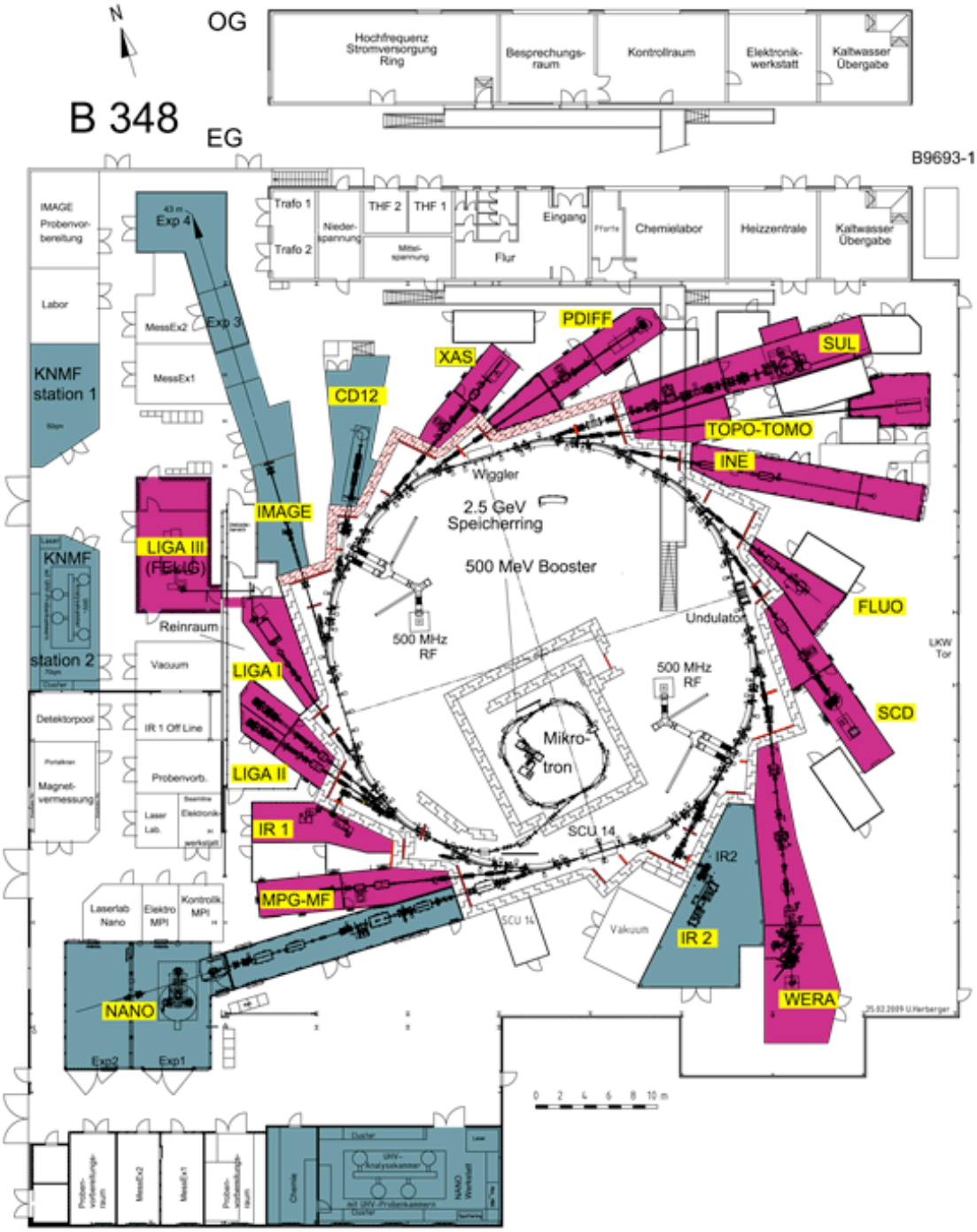

Figure 2.9: Overview over the ANKA facility. The violet beamlines are already in operation, the blue ones are being constructed at the moment.

to be stored in the ring without causing instabilities. With the new electron source that was installed very recently (Spring 2009), it is now possible to create a filling pattern with only one single bunch, which allows the study of multi-bunch and single-bunch effects in more detail. The spectrum of the incoherent synchrotron radiation which was illustrated in Figure 2.4, was calculated for the parameters of the ANKA storage ring.

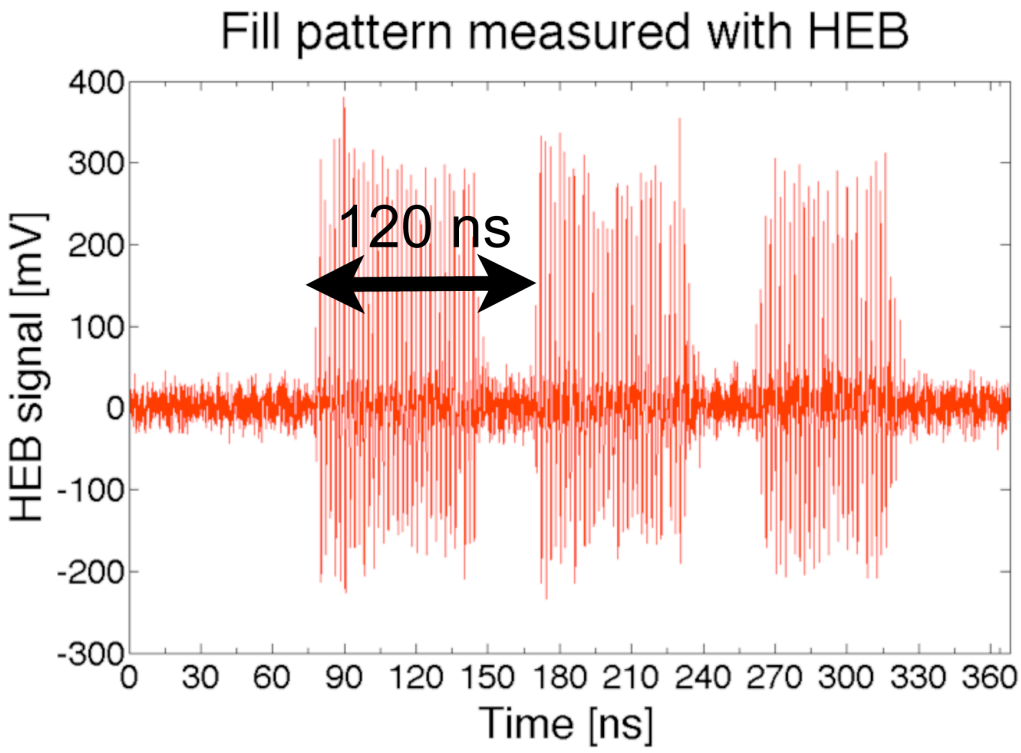

Figure 2.10: A typical filling pattern of the ANKA storage ring. The signal was recorded with a hot electron bolometer (HEB) which is a very fast THz-detector that can resolve the bunch structure which is imprinted into the synchrotron radiation. The time axis represents one revolution which takes 368 ns. There are three main structures, so called trains which show a bunched substructure of 33 bunches each, the time between the beginning of two trains is 120 ns. The actual length of the radiation pulses cannot be resolved with this detector, because it is in the picosecond range and the temporal resolution of the HEB is 1 ns.

	Normal User Operation	Low-α_c-Operation
Circumference	110 m	
Harmonic Number h	184	
RF Frequency f_{RF}	499.69 MHz	
Revolution Frequency	2.715 MHz	
Number of Bunches	3 trains a 33 bunches	
Beam Energy E	2.5 GeV	1.3 GeV
Beam Current I_{beam}	$\approx$ 150 mA	$<$ 100 mA
Critical photon energy ϵ_{crit}	6.2 keV	0.88 keV
Bunch length (RMS) σ_z	$\approx$ 10 mm (30 ps)	$\approx$ 0.3-3 mm (1-10 ps)

Table 2.1: Parameters of the ANKA storage ring.

3. Methods for Bunch Length Measurements

There are various techniques to measure the bunch length, some measure the electron bunch length directly, others measure the pulse length of the synchrotron radiation pulses. Some allow to not only measure the length of the pulses, but also their exact time profile. In general there is to say, that the shorter the pulses are, the more challenging the measurements become. Also, for very short pulses the exact temporal profile is of great interest to study bunch deformations in further detail.
In this work, the techniques which are used at the ANKA synchrotron light source, are presented. In order to validate these measurements another independent set up to measure the pulse length was investigated and tried out.

3.1 Synchrotron Tune

During the discussion of the bunch length in chapter 2.4 the synchrotron tune Q_s was introduced as the frequency f_s of the longitudinal oscillation of particles around their reference phase Ψ_s divided by the revolution frequency f_{rev}. The theoretical bunch length was given by equation 2.8:

$$\sigma_{z,\text{theo}} = \frac{c\sigma_\delta|\alpha_c - \gamma^{-2}|}{2\pi Q_s f_{rev}} \tag{3.1}$$

We can clearly see that the theoretical bunch length depends on the synchrotron tune Q_s, but there is also the momentum compaction factor in the formula which can be measured, but not with the desired accuracy. It is very interesting to measure the bunch length during the squeezing process where α_c is decreased in steps to shorten the bunch length. γ is between 980 (at 0.5 GeV) and 4900 (at 2.5 GeV) for ANKA (estimated with $\gamma \approx E/m_e c^2$ for relativistic particles), so γ^{-2} ranges between $4 \cdot 10^{-8} - 10^{-6}$ whereas α_c ranges between $10^{-4} - 10^{-2}$, so γ^{-2} can be neglected in equation 3.1, and $Q_s \cdot f_{rev} = f_s$ so equation 3.1 shortens to:

$$\sigma_{z,\text{theo}} \approx \frac{c\sigma_\delta|\alpha_c|}{2\pi f_{s,\text{theo}}} \tag{3.2}$$

The theoretical synchrotron frequency $f_{s,\text{theo}}$ is given by [14]:

$$f_{s,\text{theo}} = f_{\text{rev}} \sqrt{\frac{\alpha_c h}{2\pi E} \sqrt{(g \cdot e \cdot V_{\text{RF}})^2 - (U_0 + k)^2}} \tag{3.3}$$

Where E is the beam energy, g a voltage calibration factor, U_0 the losses in the dipoles and k higher order losses.

From equation 3.3 it can be seen, that $\alpha_c \sim f_s^2$. Placing this relation in equation 3.2 where we have $\sigma_z \sim \frac{\alpha_c}{f_s}$, we get $\sigma_z \sim f_s$, with which we can rewrite equation 3.2:

$$\sigma_{z,\text{real}} = f_{s,\text{exp}} \frac{cE\sigma_\delta}{f_{\text{RF}} f_{\text{rev}} \sqrt{(g \cdot e \cdot V_{\text{RF}})^2 - (U_0 + k)^2}} \tag{3.4}$$

This equation allows us to extract the bunch length out of the synchrotron tune, during the squeezing process. The synchrotron tune itself can be measured with a spectrum analyser, which gets its signal from a so called stripline pick up. The stripline consists of a set of small metalstrips in the beam pipe in which a signal from the electron beam passing by is induced. Looking at this signal in the frequency domain one sees side bands with the distance of synchrotron frequency from the main peak of the revolution frequency (or of its higher harmonics). A spectrum recorded with a spectrum analyser can be found in Figure 3.1.

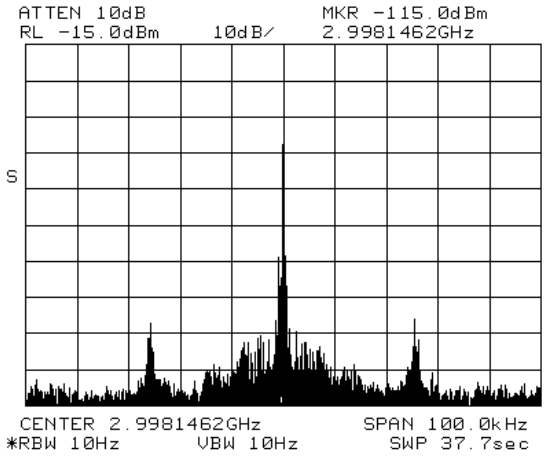

Figure 3.1: Spectrum recorded with a spectrum analyser. The centre peak resembles a higher harmonic of the revolution frequency, the side bands are synchrotron side bands and their distance from the centre peak is the synchrotron frequency.

3.2 Streak Camera

Streak cameras are used to record very fast processes. They can be used in many different fields where processes occur on a very fast time scale (resolution down to a few ps). A few examples are given in [15]. Soon streak cameras were utilised in the field of accelerator physics to analyse the time profile of synchrotron radiation pulses in the visible range. There are a lot of different types and set up opportunities of streak cameras tailored for

the different applications, the set up used at the ANKA storage ring will be explained.

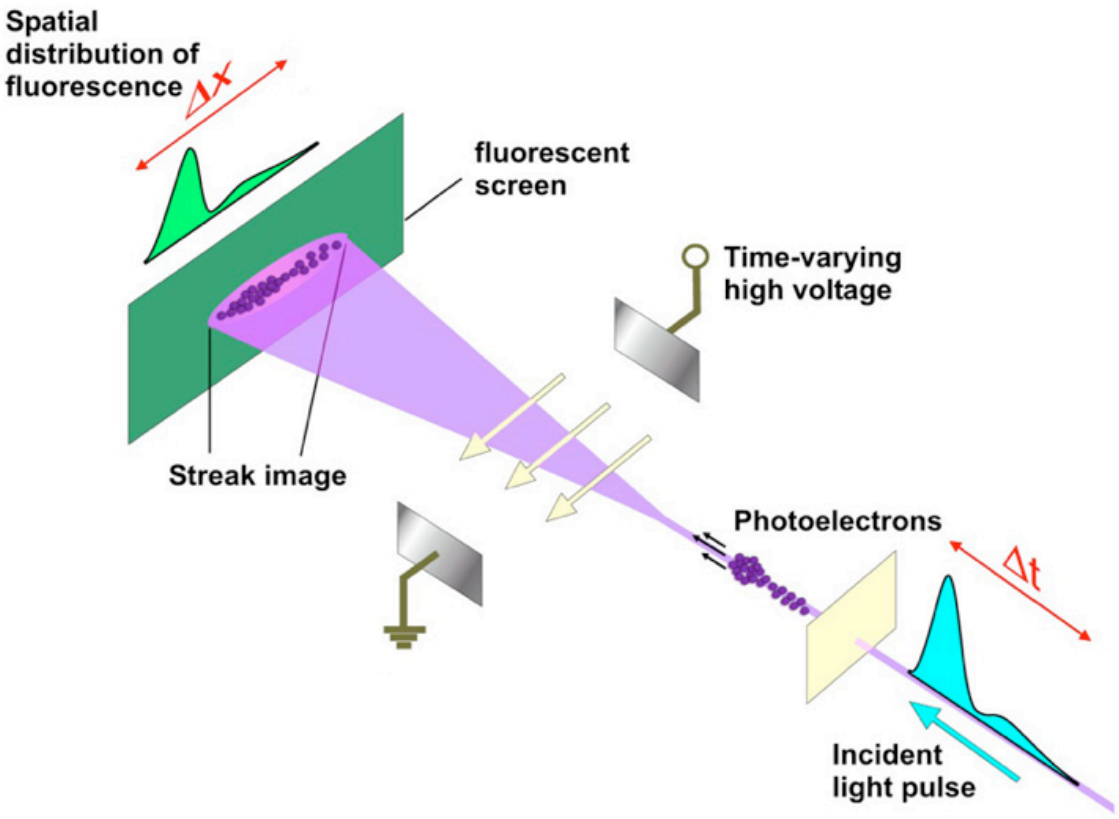

Figure 3.2: Schematic drawing of the working principle of a streak camera [16].

The working principle of a streak camera is depicted in Figure 3.2: An incident light pulse is sent to a photocathode which results in photoelectrons being emitted from the photocathode. The time distribution of those photoelectrons is equal to that of the incident light pulse. The photoelectrons are then directed towards a fluorescent screen. On their way to the fluorescent screen they have to pass a time-varying high voltage field between two metal plates, this is usually referred to as sweep field. The sweep field will be set in a way that electrons arriving earlier will see a different field than electrons arriving later, which will then in turn result in them hitting the fluorescent screen at a different location. There is an electron multiplier (MCP) right before the fluorescent screen to amplify the signal (not drawn). The streak image will have a spatial distribution along the screen that corresponds to the time distribution of the incident light pulse. A CCD camera is used to capture an image of the fluorescent screen to allow evaluation of the data. With this set up not only the pulse length, but also the full time characteristics of the pulse can be extracted from the CCD image.

The synchrotron radiation has an intensity distribution which corresponds to the charge distribution within the accelerator. For ANKA it was already explained in chapter 2.6 that this can vary between a bunch-train structure with usually three trains consisting of around 30 bunches each or just a single bunch every revolution (time for one revolution:

368 ns). Especially during the multi-bunch operation it is of great interest to not only measure the length and shape of bunches, but also the time structure during one whole revolution. This, however, brings another challenge with it: The bunches itself are very short (ps) compared to the distance between two bunches (2 ns). So to measure the filling pattern a time scale with several hundred nanoseconds is required, but to measure the length of the pulses themselves, a fine picosecond-resolution is needed. This can be achieved by adding a second sweep unit with a field perpendicular to the first one, so the two dimensional fluorescent screen can be filled not only in x-direction, but also in y-direction. This second sweep unit then sweeps at a different speed, thus allowing us to have a slow and a fast time axis on the screen.

For the streak camera in use at the ANKA storage ring (model C5680 by Hamamatsu) the fast time axis can be varied between 190 ps and 800 ps in four steps, the slow time axis can be varied between 100 ns and several milliseconds. The horizontal and vertical size of the light beam which is focussed onto the slit opening of the streak camera is one of the factors limiting the resolution along the axes, which can be seen in Figure 3.2, where the image on the screen is already two dimensional without having a sweep unit in the second direction, so this limits the resolution.

The scale along the fast time axis is up to 800 ps, as stated above, but the actual pulse length of the synchrotron radiation pulses is below 100 ps, and can be even as low as a few picoseconds during the low-alpha operation. This means there is quite some unused space along the fast axis whereas the time resolution along the slow time axis which can only go as low as 100 ns is barely enough to tell two bunches apart when the smearing because of the beam size is taken into account. It is very convenient to have two neighbouring bunches detected on the slow time axis, so the odd bunches are for example shown in the bottom half of the screen and the even bunches in the top half (or the other way around, depending on the delay time chosen). In order to achieve this a 250 MHz sine wave signal is used ($\frac{1}{2} \cdot f_{RF}$) to control the fast sweeping unit. The delay time is then adjusted that, out of two neighbouring bunches, one lies on the rising slope of the trigger signal and one on the falling slope. Changing the phase between the trigger signal and the actual sweep allows us to move the bunches further apart along the fast time axis.

By decreasing the horizontal and vertical aperture of the streak camera the time resolution can be improved, this is, however, at the cost of intensity. With a lower intensity the image on the screen is less bright and with just a single shot, the evaluation of the data might not be possible, then averaging has to be done. The averaging can either be done by recording sequences of many single shots and summing them up, or directly on the fluorescent screen by irradiating it for a longer time. Both methods have the disadvantage that the pulse length smears out because of variations in the arrival time of the pulses, which are mainly due to the synchrotron oscillation. When recording sequences, the range of the slow time axis has to be set to several μs (usually around 100-500 μs) to obtain a sufficiently high signal to allow an evaluation. At this rather long range the signal from all bunches is depicted for many revolutions (more than 1300 revolutions for a time range of 500 μs). An example of a single image from such a sequence can be found in Figure

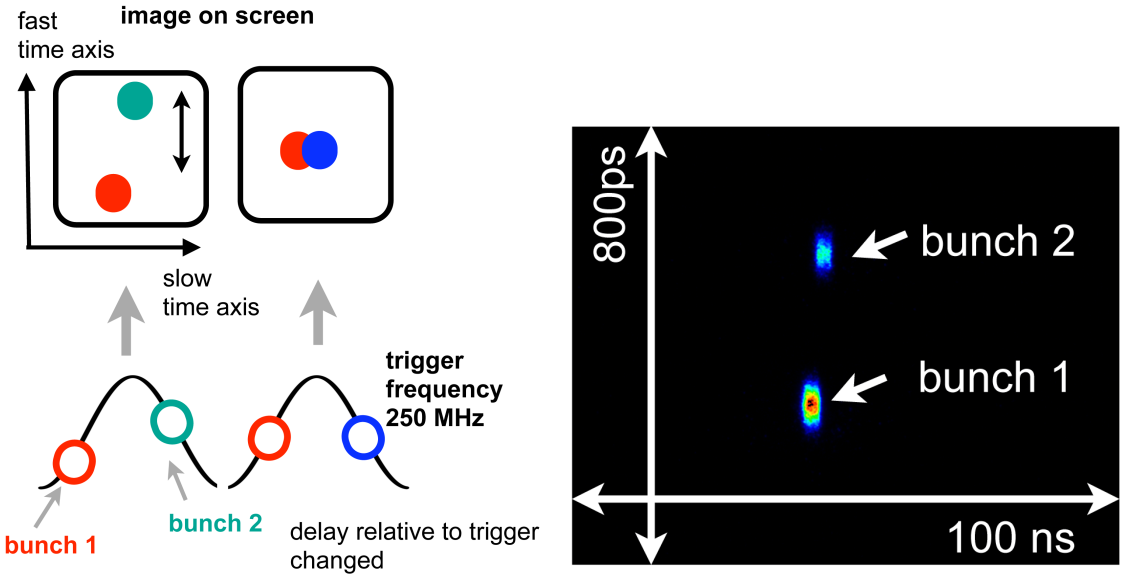

Figure 3.3: Left: Schematic drawing to illustrate how consecutive bunches can be depicted with a streak camera when the delay time relative to the trigger frequency is changed. Right: Actual image recorded with the streak camera at ANKA, showing two bunches.

6.2. The electrons created by photons from different bunches overlap slightly which leads to a broadening of the extracted pulse length when oscillations are present. This effect is decreased significantly during singlebunch-operation, because there the time between two consecutive bunches is not 2 ns but 368 ns, in addition to that the current per bunch can be slightly higher which leads to a stronger signal from single pulses.

3.3 Field Autocorrelation with Coherent THz-Radiation

Another method, which is used at ANKA to determine the pulse length is the field autocorrelation of coherent THz-radiation. Figure 3.4 shows a field autocorrelation recorded for a coherent THz pulse emitted during the low α_c operation at ANKA [17]. The recording was done with a Michelson interferometer at the IR1 beamline. The detection was accomplished with a Bolometer (radiation detector sensitive to THz-radiation). Because of the fact that the radiation is coherent, the pulse length can be extracted from the field autocorrelation (further information about field autocorrelations can be found in chapter 4.2). From the data taken, the FWHM pulse length of the coherent THz pulse was found to be only 1 ps, however the tune measurement predicted a significantly longer bunch length. A possible explanation could be that only a part of the bunch emits coherently, so the pulse length of the coherent THz-pulse is smaller than the actual bunch length. It is also possible that the electron bunch develops some kind of sub-structure (micro-bunching), which then leads to further changes of the interferogram. Another problem is that the spectrum of the radiation is changed by different optical components of the beamline such as windows and the beamsplitter in the interferometer. All of these effects have to be studied and the recorded data has to be corrected accordingly to allow a detailed evaluation. This method, however, is very powerful, especially, for the users who want to work

with the emitted coherent synchrotron radiation, it is important to know and understand all the characteristics of the radiation they get at the beamline. This method has to be investigated in greater detail and this is also work in progress within the THz group at ANKA.

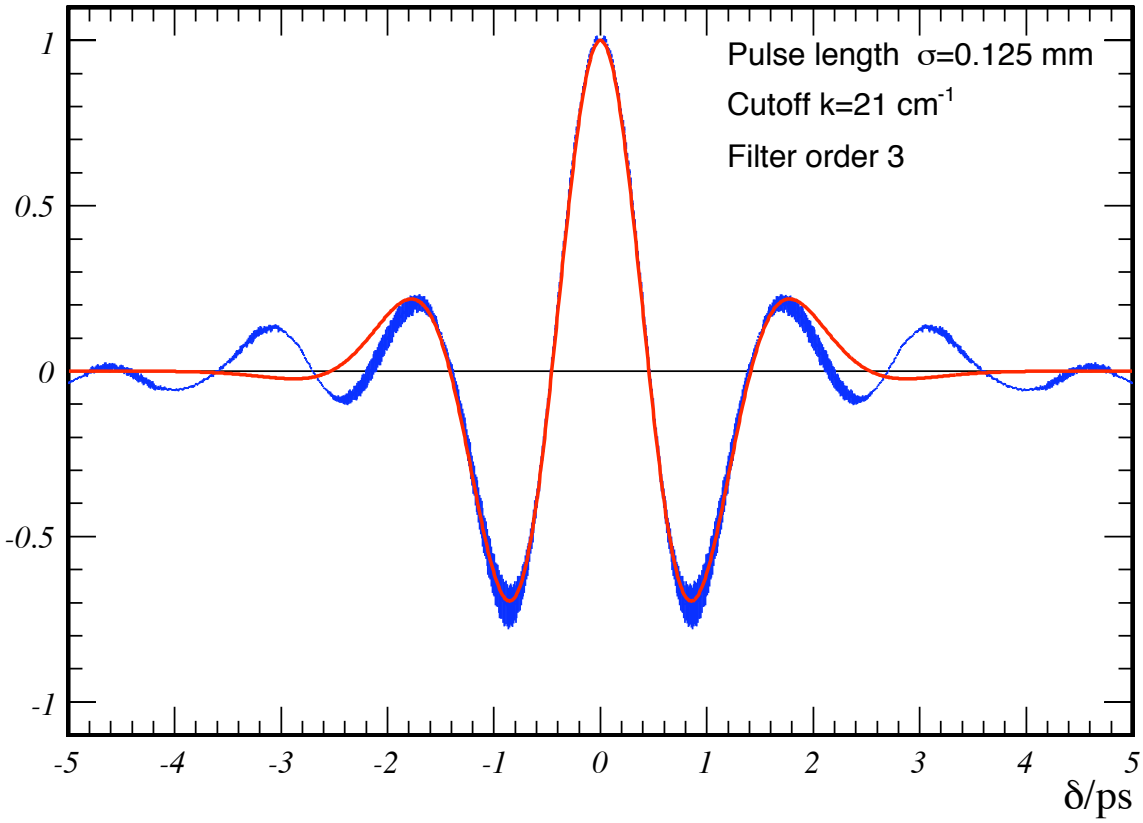

Figure 3.4: Field autocorrelation trace of a coherent THz radiation pulse, recorded with a Michelson interferometer at ANKA [17]. The x-axis shows the delay in ps, the y-axis shows the signal strength in arbitrary units. The red curve shows a fit to the recorded data (blue). The recorded data has been symmetrized, and filled into a profile histogramm. $\sigma = 0.125\,mm = 0.417\,ps$, so for a Gaussian pulse shape the FWHM would be around 1 ps.

4. Optical Autocorrelation

Optical autocorrelation is a technique commonly used to determine main characteristics of pulsed laser beams, such as pulse length and the spectrum [18]. However, this technique is not limited to pulsed lasers but can also be used to characterise synchrotron light pulses [4].

4.1 General Properties of Autocorrelations

Mathematically speaking, an autocorrelation is a special case of cross-correlation. A cross-correlation is used to compare two complex, square-integrable functions with each other, at a delayed time/location. This is achieved by forming their inner-product:

$$(f \star g) = \int_{-\infty}^{\infty} f^*(t)g(t+\tau)dt \tag{4.1}$$

In the case of an autocorrelation the two functions are identical:

$$A_f(\tau) = \int_{-\infty}^{\infty} f^*(t)f(t+\tau)dt \tag{4.2}$$

There are a few noteworthy properties of an autocorrelation function [19]:

- It is always symmetrical in τ.
- Its maximum lies at $\tau = 0$.
- If $f(t)$ has a periodicity, then this periodicity is conserved in $A_f(\tau)$.
- The autocorrelation of the sum of two functions can be rewritten as the sum of the autocorrelations of each of those functions plus their cross-correlations.
- Phase information is lost during the autocorrelation because only the square of the function is taken into account, hence making it a non-reversible operation.

4.2 Optical Autocorrelation

In the case of optical autocorrelation, the function is a time dependent wave function and τ is a time delay introduced to that function.
There are different types of optical autocorrelations, depending on which kind of variable is being measured. The most basic form is the field autocorrelation where E(t) is the electric field of a photon beam:

$$A^{(1)}(\tau) = \int_{-\infty}^{\infty} E^*(t)E(t+\tau)dt \tag{4.3}$$

It is often being referred to as first order autocorrelation. The Fourier transform of the field autocorrelation returns the spectrum of the radiation. Depending on the characteristics of the radiation further information can be extracted from the spectrum. For example, for Fourier-limited radiation pulses the time-bandwidth-product is constant, so a pulse can be characterised by either measuring its spectral width or its temporal width [19].

The intensity autocorrelation, where $I(t) = |E(t)|^2$,

$$A^{(2)}(\tau) = \int_{-\infty}^{\infty} I(t)I(t-\tau)dt \tag{4.4}$$

holds information about the pulse length if the original pulse shape is known. Usually the FWHM is used to describe the pulse length. Figure 4.1 gives examples of intensity autocorrelation signals obtained for different initial pulse shapes.

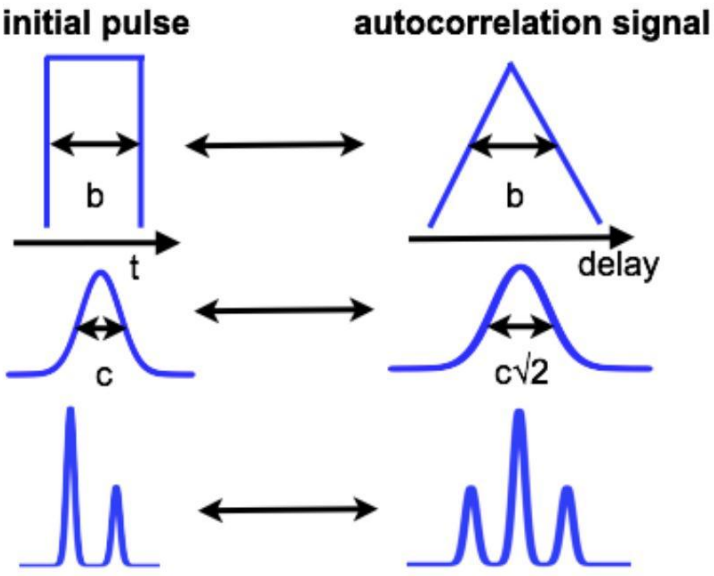

Figure 4.1: Comparison of the autocorrelation signals obtained from different initial pulse shapes: Top: Rectangular pulse yields triangular autocorrelation. Middle: Gaussian pulse remains Gaussian but widens by a factor of $\sqrt{2}$. Bottom: A series of two Gaussian pulses is turned into an autocorrelation with three peaks, the distance between peaks is conserved and the peaks itself widen in the same way as shown in the middle picture.

With a known pulse shape the deconvolution factor, which connects the FWHM of initial pulse and that of the autocorrelation signal, can be calculated. For a Gaussian pulse this factor is $\sqrt{2}$. In [19] (Table 12.1 on page 944) a list of deconvolution factors for different pulse shapes can be found.

4.3 Experimental Realisation

An optical autocorrelation is performed with optical beams (usually laser beams). The beam is split into two beams with a beamsplitter. A variable delay is introduced in one of the split beams, then they are recombined and focused on a detector. The signal on the detector in dependance of the delay is measured. This is illustrated in Figure 4.2

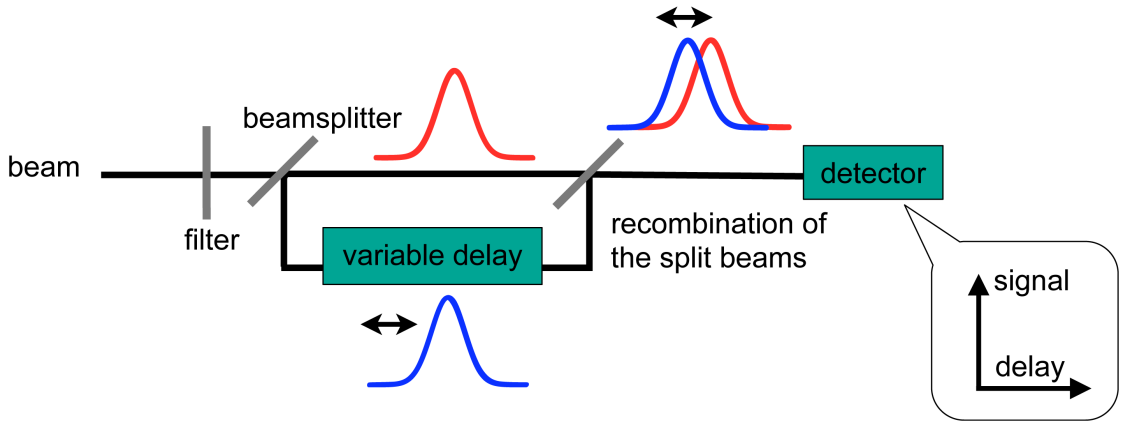

Figure 4.2: Sketch of the experimental realisation of an autocorrelator.

In the following two sub-chapters there will be a more detailed description of the possible optical set up and the detector choices.

4.3.1 Optical Set up

The most common optical set up used for an autocorrelator is that of a Michelson-type interferometer (depicted in figure 4.3), where a beam splitter is used to split the beams and then recombine them again as well. The beam splitter must be optimised for the wavelength range of the beam. The best beam splitters for optical autocorrelations reflect 50% of the intensity and transmit 50% (ignoring absorption losses). One of the split beams is reflected back onto the beam splitter by a fixed mirror where half of it gets transmitted back into the source and the other half gets reflected onto the detector. The other split beam hits the movable mirror instead and half of it reaches the detector and the other half is reflected back into the source. The movable mirror must be mounted on a translation stage which can be moved over a distance corresponding at least to the pulse length with sufficient granularity (e.g. 1 ps$\cdot c$ = 0.3 mm). The Michelson-type set up is referred to as collinear set up because the beams travel on top of each other after the recombination. This set up is rather easy to build and requires only few optical parts. Its downside, however, is that at least 50% of the initial intensity is reflected back into the source and never reaches the detector.

In the non-collinear set up the variable delay is introduced slightly differently rather than reflecting the beam directly back with one mirror on a translation stage, the beam is reflected back with a slight offset, which is usually achieved by a roof-mirror on a translation stage. The recombination of the two split beams is then achieved with a lens (parallel rays falling onto a lens meet in its focal point). This set up is more challenging to build and to align, since there are more optical parts needed. Especially the recombination requires very precise alignment, because the two beams will only meet in one point, the focal point of the lens. This is exactly where the detector must be placed.
The collinear and non-collinear set up possibilities are illustrated in Figure 4.3

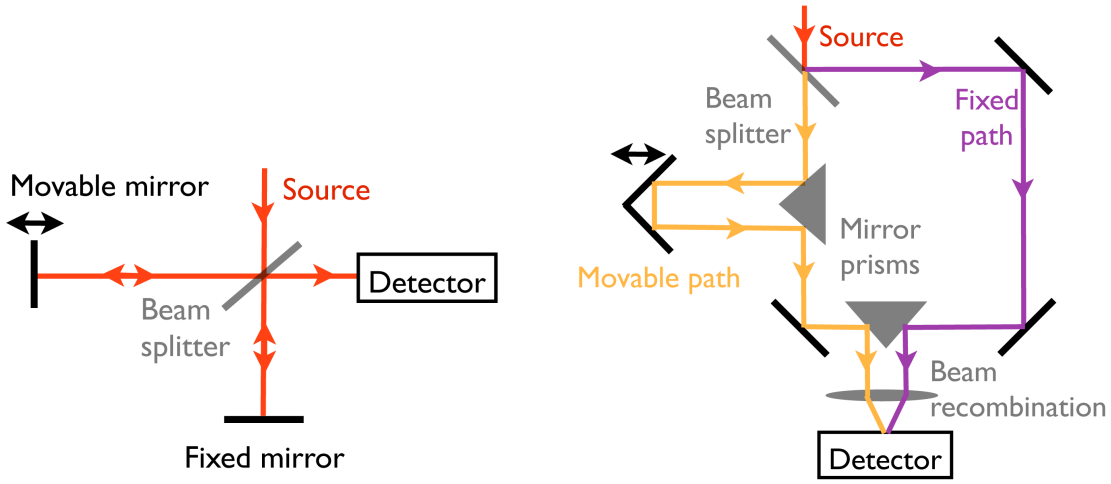

Figure 4.3: Left: Collinear set up which is often referred to as Michelson-type autocorrelator. Right: Non-collinear set up which uses a lens to recombine the split beams.

4.3.2 Detector

There are different requirements for the detector, depending on what kind of autocorrelation signal is planned to be observed. For a field autocorrelation a detector with a linear response to the intensity of the radiation is required. To perform an intensity autocorrelation a detector that is sensitive to the square of the incident intensity is required. This can be seen by looking at equation 4.4. There are two rather commonly used non-linear processes that can be used for non-linear detectors:

- Second harmonic generation (SHG) in non-linear crystals
- Two-photon absorption processes (TPA) in semiconductors

Both of them are two-photon processes and hence have a few characteristics in common. The number of two-photon processes N_p, for example, can be expressed as:

$$N_p \propto \frac{I^2}{\sigma_x \tau}, \tag{4.5}$$

where I is the intensity of the incident radiation, σ_x is the spot size of the beam and τ stands for the pulse length. Equation 4.5 shows that two-photon processes are proportional

to the square of the intensity, so basically to the square of the number of photons involved. Their number is also inversely proportional to the beam size and the pulse length, this is because two photons need to be close together in time and space in order to interact with each other. However this equation only holds for reasonably short pulse lengths, because the longer the pulses get, the less likely it is that a photon from the front of a pulse can create a TPA process with one from the back, so N_p strives to a minimum constant value of for a continuous beam.

For practical use, the following relation is given: The signal of the detector I_{det} is proportional to the peak optical power times the average optical power [18]:

$$I_{det} \propto P_{peak} \cdot P_{avg} \tag{4.6}$$

Second harmonic generation is sometimes called frequency doubling: Two incident photons are combined to one photon with twice the energy. This process can occur in non-linear crystals such as beta barium borate (BBO). Incident light of wavelengths between 410 nm and 3500 nm can be phase matched, depending on the tilting angle of the crystal (different wavelengths require different incident angles to allow SHG). The frequency doubled light is then detected with a standard photodiode sensitive to its frequency. In order to remove the unwanted background signal, a non-collinear set up is of advantage. The incident beams hit the crystal under different angles, which means that only frequency doubled photons which are created by one photon from beam A and one photon from beam B leave the crystal in the direction the photodetector is placed. An illustration of this background free set up can be found in Figure 4.4. The photodetector detects a signal that is linear to the incident frequency doubled light, however the intensity of the frequency doubled light itself is proportional to the square of the intensity of the original incident light, thus enabling the measurement of an intensity autocorrelation.

Two-photon absorption processes work the following way: A photon hitting a semiconductor can create a free carrier pair if its energy is large enough to cross the band gap (if not its energy is transferred into phonons). However there are also processes of higher order where not only one, but two (or even more) photons are absorbed at the same time and location, they can then also create a free carrier via a virtual intermediate state if the sum of their energies is greater than the band gap. Of course, those processes are a lot less likely than the direct absorption processes, so it has to be made sure that there are no photons which could cross the band gap on their own in order to lower the background. For sources with a wide spectrum filters need to be applied and for lasers one has to pick a semiconductor with a band gap that is larger than the photon energy but smaller than twice the photon energy.
Generally these TPA processes happen in every semi-conductor, so the choice of detectors ranges from photodiodes [20] over LEDs (light emitting diodes) [21] [22] to photomultiplier tubes (PMTs) [23]. Measurements with other semiconductor detectors can be found in the literature [24] [25] [26] [27] [28] [29]. The sensitivity of different LEDs and a photodiode has been investigated in the framework of this thesis.

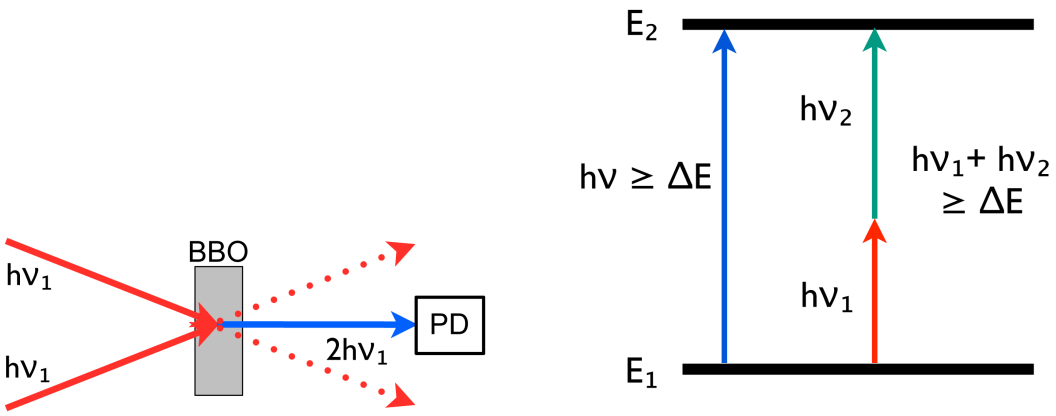

Figure 4.4: Left: SHG in a non-linear crystal (e.g. made out of BBO = beta barium borate) Right: Single photon absorption and TPA processes in a semiconductor.

5. Autocorrelation Measurements

In the framework of this thesis, the feasibility of an intensity autocorrelation with semiconductor detectors that would allow the measurement of the pulse length of the synchrotron radiation, was investigated. In the following paragraph the experimental approach is summarised. A more detailed presentation and discussion of the results can be found in the next sections of this chapter.

The first test measurement was carried out with a fs-laser (λ = 800 nm) from Gigaoptics (GigaJet 20). For the optical set up only components which were already present have been used and the measurement was done with the same type of red GaAlAs LED (ΔE = 660 nm) that had been used by Reid et al. [22], also a similar green LED (ΔE = 425 nm) had been tried out. The set up was very basic and most of the components were not optimised for the wavelength of the laser. Several autocorrelation traces were recorded for the red LED and the beam was attenuated to a lower intensity to see how sensitive the set up was. At an optical power of roughly 6 mW no clear autocorrelation trace could be seen anymore. For the green LED, the signal was significantly lower and no autocorrelation trace could be recorded. The beamsplitter which unfortunately had a transmission to reflectance ratio of 70:30 and not 50:50 was designed for the visible range only. This caused multiple reflections which caused the main pulse to be split into one pulse being followed by a second not so bright pulse at a delay of two times the thickness of the beamsplitter at an incident angle of 45°, this caused the autocorrelation trace to exhibit three peaks instead of one (see figure 4.1 for further explanation).

The optical power at the diagnostic beam port at the IR1 and IR2 beamlines at ANKA was measured to get an estimate for the properties of the source which should be used later on. The optical power at the IR2 beamline, which is currently in the commissioning phase and not yet open for users, was found to be higher by a factor of 3.6 in the desired wavelength range. Also the linear dependence of the optical power from the beam current which was stated in equation 2.3 was experimentally validated (see Section 5.7.1).
The first attempt to measure the pulse length with the synchrotron light did not yield the

desired results, so an optimization of the set up was undertaken.
The detector was prepared slightly differently: The LED was glued into an aluminium ring and the dome of the LED was then cut off and the surface was repolished. This allowed easier mounting. In addition to that a GaAsP photodiode (G1118 from Hamamatsu) with a band gap that is similar to that of the red LED was bought to find out whether it would be more sensitive. A lemo instead of a BNC connector was used to connect the detector to the amplifier, since previous tests had shown, that with a lemo cable there was less noise on the signal. Instead of feeding the signal directly to the lock-in Amplifier, the signal was first amplified by a current to voltage amplifier (Model 428 from Keithley). This amplifier picked up a lot of noise from the power network, so the pre-amplified signal was then fed to the lock-in amplifier to filter out this noise. The readout of the signal was done with LabView which allowed the access of a server to log important beam parameters (beam current, energy, beam position, RF voltage, RF frequency etc.) simultaneously. The optical set up could greatly be enhanced by using a beam splitter that is designed for the near infrared region (NIR) with a 50:50 transmittance to reflectance ratio. Also new mirrors were acquired which have a better reflectivity in the desired wavelength region. The translation stage was exchanged for a 150 ps - ScanDelay from APE [30]. Both a collinear and a non-collinear set up were tried out. The non-collinear set up had the great advantage of not losing 50% of the intensity right away, but the recombination of the split beams with a simple lens (the aperture of the microscope objective was too small to be used) did not focus down the beam well enough. Furthermore it was nearly impossible to reach a good overlap of the two beams. So for the final set up a collinear alignment was chosen.

After all these improvements, further measurements with the synchrotron light still did not yield the desired results. Another laser test measurement was carried out at the Ruhr University of Bochum, where an autocorrelation measurement with an LED as detector for one of their fs-lasers had been carried out a few years ago [31]. A full discussion of the results can be found in section 5.2. A collinear set up was chosen as the final one. Studies regarding the lower intensity limit and the characteristics of the different detectors have been carried out. A great achievement in sensitivity could be achieved and the set up could be aligned very precisely. Autocorrelation traces from which the pulse length could be extracted were visible down to optical powers of as low as 150 μW. The signal to background ratio could be increased to values as high as 18:1 by using a different chopper set up, which is explained in more detail in section 5.4. The whole set up was then moved back to ANKA and final measurements with the synchrotron light were undertaken. The predictions derived from the results obtained during these test measurements stated that the optical power of the synchrotron radiation was too low by a factor of two. In theory, this could still allow to see an indication of an autocorrelation trace, however such a hint was not seen in the experimental data.

5.1 Extraction of the Initial Pulse Length from the Autocorrelation Trace

To extract the FWHM value of the initial pulse length from the measured autocorrelation curves, the following steps were undertaken: The initial pulse shape was assumed to be Gaussian, therefor the shape of the autocorrelation was fitted by the following function of Gaussian type:

$$f(x) = a_1 \cdot \exp\left(-\left[\frac{x-b_1}{c_1}\right]^2\right) + c \tag{5.1}$$

Here the variance σ^2 is $\left(\frac{c_1}{\sqrt{2}}\right)^2$. For Gaussian pulses the FWHM and the standard deviation σ are related the following way:

$$\mathrm{FWHM}_{Gaussian} = 2 \cdot \sqrt{2\ln 2} \cdot \sigma \approx 2.35\sigma \tag{5.2}$$

The FWHM of this function is $2 \cdot \sqrt{\ln 2} \cdot c_1$. The FWHM of the initial pulse τ_i is shorter by a factor of $\frac{\sqrt{2}}{2}$ (the deconvolution factor) than the FWHM of the autocorrelation trace. This gives us the following relation for τ_i in dependance of c_1:

$$\tau_i = \sqrt{2 \cdot \ln 2} \cdot c_1 \approx 1.18 \cdot c_1 \tag{5.3}$$

In order to make an assumption of the error of the fit, the data was binned in a profile histogramm with ROOT[32], the fit was performed with an x-error of half of the bin-width and the y-error was adjusted till the χ^2/NDF (NDF is the number of degrees of freedom, so the number of bins minus the number of fit parameters) was approximately 1. This was done in order to get a realistic uncertainty for the results. An example for such a fit can be found in Figure 5.1. The signal of the scanner position displayed some kind of hysteresis. The recorded curves for a forward movement of the scanner have a slight delay in X-direction in respect to the ones recorded when the scanner moves in the other direction. Therefor the data sets recorded in one direction and the other direction were evaluated separately.

5.2 Data Sets Recorded with a fs-Laser

During a one week measurement time at the Institute of Physical Chemistry II at the Ruhr University of Bochum, the main goals were to find a lower sensitivity limit of the set up, but also to do further studies on the different detector possibilities.
Autocorrelation traces have been recorded with a GaAsP photodiode and two different GaAlAs LEDs (one had 2800 mcd and one had 1000 mcd) as detector. The measurements were done at different optical input powers and the lower sensitivity limit was found experimentally for the photodiode and the LED with 2800 mcd. Different scan speeds (speed at which the delay is changed) and different amplification factors and recording times have been tried out to find the best settings. Alignment difficulties and the reproducibility of measurements were studied. The effects of dispersion in media were examined by placing an extra-glass block in the beam path to elongate the pulses.

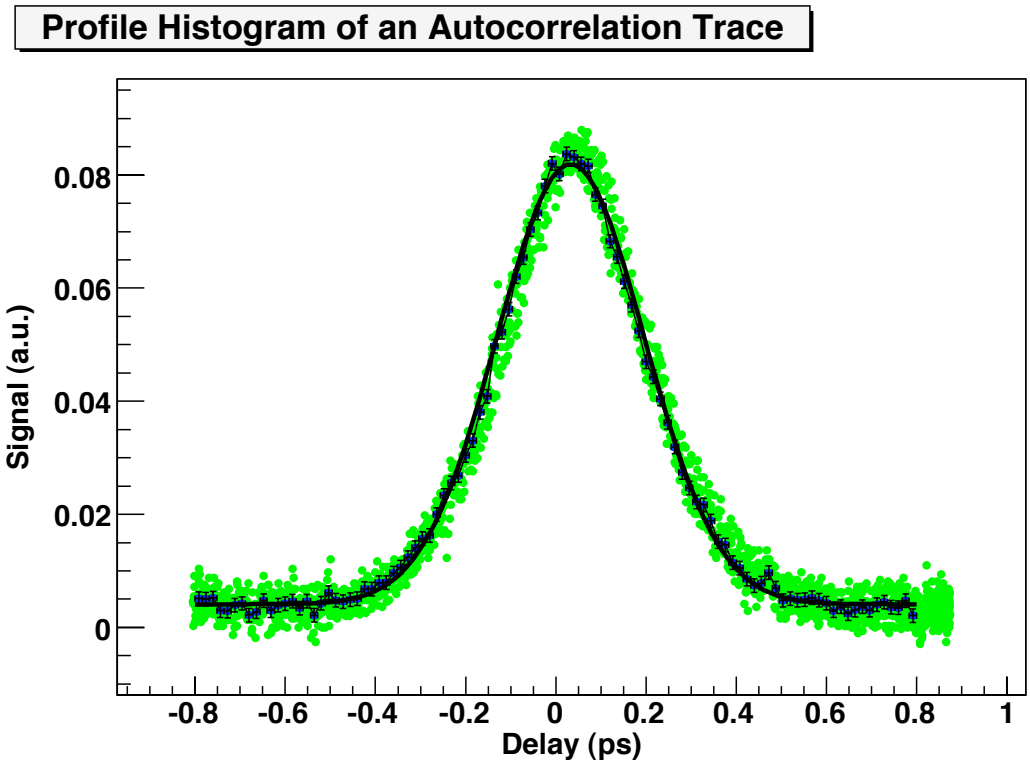

Figure 5.1: Example of a profile histogram of an autocorrelation trace recorded with a GaAsP photodiode at an optical input power of 0.5 mW.

5.3 Set Up

The set up had already been built up and had been pre-aligned with an alignment laser. It was then transported to Bochum, where it was connected to a fs-laser from Gigaoptics (GigaJet TWIN, 50 fs pulse length, 800 nm central wavelength, 1 GHz repetition rate). The set up used in detail is depicted in Figure 5.2. The readout of the signal from the lock-in amplifier was connected to an AD-converter (Model USB-6221 BNC from National Instruments) which allowed the digitalisation of the data and logging with LabView. The position of the mirror, which was given by an output signal from the delay scanner was read out as well and converted to a delay in ps. The optical input power was measured with the same powermeter (PM-100 from Thorlabs for optical powers up to 2 mW) that had been used for all optical power measurements previously undertaken at the ANKA storage ring. For optical input powers of more than 2 mW a powermeter with a thermal sensor was used, which had a rather poor power resolution for optical powers of less than 10 mW. The optical power was measured right before the beams pass through the microscope objective.

5.4 Background Reduction

Unless an intensity autocorrelation is set up to be background free, which can only be achieved with non-linear crystals (see chapter 4.3.2), a certain background level limits the peak signal to background ratio. This background comes from the fact that TPA

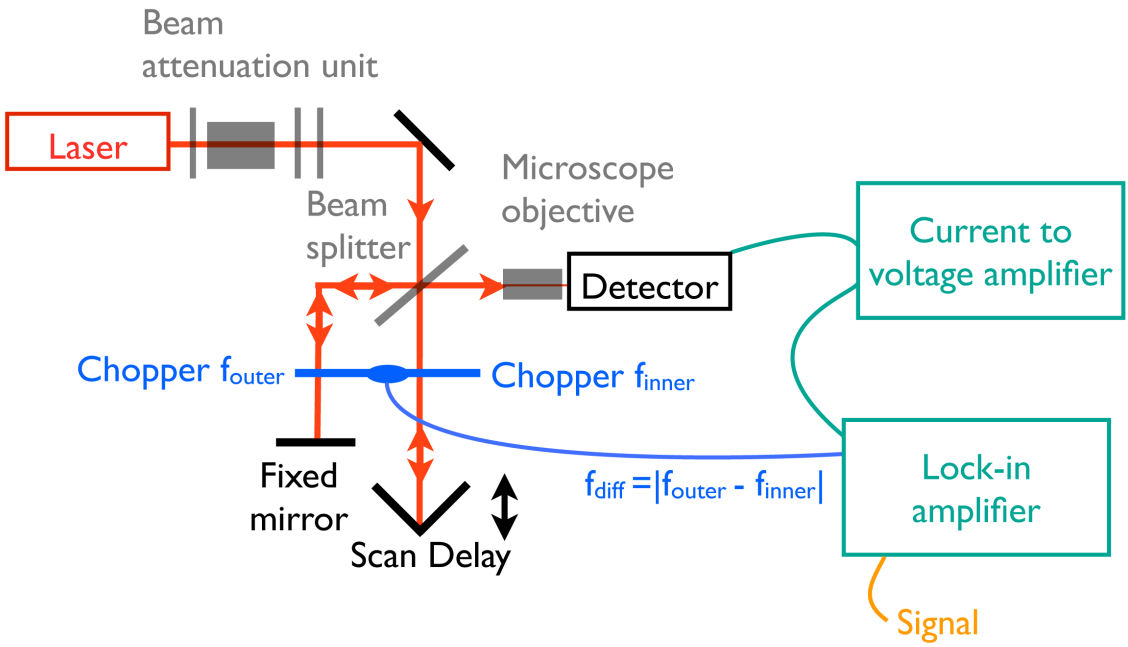

Figure 5.2: Sketch of the set up used with a Gigaoptics fs-Laser at the Ruhr University of Bochum. The "beam attenuation unit" consists of a zero order quartz retarder (half-wave plate), a beam cube polarizer, a neutral density filter wheel and a 780 nm long pass filter. The chopper which was used had six holes on the outer part of the wheel and only five holes on the inner part, so two different chopping frequencies could be achieved. The chopper control unit then produced a trigger signal with the difference frequency.

processes can also occur between two photons of the same beam. The raw-signal of an intensity autocorrelation with background is [21]:

$$S_2(\tau) = \int_{-\infty}^{\infty} \left|(E_1(t) + E_1(t+\tau))^2\right|^2 dt \tag{5.4}$$

$$\begin{aligned} &= \int_{-\infty}^{\infty} \left|(E_1^2(t) + 2E_1(t)E_1(t+\tau) + E_1^2(t+\tau)\right|^2 dt \\ &= 2\int_{-\infty}^{\infty} I_1(t)^2 dt \\ &+ 4\int_{-\infty}^{\infty} I_1(t)I_1(t+\tau)dt \\ &+ 4\int_{-\infty}^{\infty} (I(t) + I(t+\tau))Re(E_1(t)E_1^*(t+\tau))dt \\ &+ 2\int_{-\infty}^{\infty} Re(E_1^2(t)E_1^{*2}(t+\tau))dt \end{aligned} \tag{5.5}$$

The first term in this expansion is a constant non-linear signal created by photons from within one of the beams, the second term is just the intensity autocorrelation. The third term is a slightly modified version of a field-autocorrelation, which was introduced in 4.2. The forth term represents interference fringes which are present in an interferometric autocorrelation. The last two terms both exhibit fast oscillating components (fast in respect to the oscillation of the other components).

Due to the continuous movement of the mirror and the averaging time of the lock-in amplifier which were used for the set up, these oscillations were averaged out, then the signal to background ratio $\frac{S_2(\tau=0)}{S_2(\tau=\infty)}$ can be calculated. This leaves a signal with a signal to background ratio of 3:1 (for the intensity autocorrelation without interference fringes).

In reality the signal to background ratio would be even lower because the overlap of the two beams has to be taken into account as well. There is also a contribution which is created by single photons being absorbed and creating a free carrier pair. This can happen because of doping impurities allowing single photons to create a free carrier even though their energy is below that of the band gap.

In order to reduce the background signal a chopper coupled with a lock-in amplifier can be used. A chopper is a device that chops the beam at a certain frequency. This frequency is fed to the lock-in amplifier along with the raw signal from the detector. The lock-in amplifier searches the raw signal for a signal that is periodic with the given frequency, the background is then subtracted.

If the chopper is placed before the autocorrelator, the signal to background ratio remains unchanged, unless there is background light. If it is placed in the path of beam A (or beam B) only, the constant signal from beam B will be subtracted as background, thus increasing the signal to background ratio.

However this can be improved even further if both beams are chopped at different frequencies and the difference frequency is fed to the lock-in amplifier [33]. Then the contribution of TPA processes from photons within beam A and beam B, along with any linear contribution, will be treated as background signal. In theory, this removes the background of the amplified signal completely. On the downside, however, the average intensity (not the peak intensity) is reduced, because the time frame during which both beams hit the detector at the same time is shorter. For the set up presented in this work, a special chopper with an outer and inner blade was used. The outer blade has six holes whereas the inner one has only five holes, therefor the difference frequency is just the revolution frequency of the whole chopper blade. When only one beam is chopped the average intensity hitting the detector is cut in half, because the chopper is closed just as long as it is open (per revolution 6 times open for 1/12th of a revolution). If, however, our chopper with five and six holes is used then the average intensity of our desired signal will be decreased to $\frac{1}{12}$ (open only once for 1/12th of a revolution).

The signal to background ratio was obtained. To account for negative background values which can occur due to the lock-in settings the measured data values were squared before fitting a Gaussian to obtain the fit parameters for the peak signal and the background level. The square root of the obtained ratio was taken as signal to background ratio. For the GaAsP photodiode a value of 18 and for the GaAlAs LED a value of 7 was obtained at an optical power of 10 mW. This shows that this method works well to increase the signal to background ratio, which was previously limited to 3:1.

5.5 Influences on the Measured Pulse Length

The Gaussian fs-pulses from a Ti:Sapphire laser are Fourier transform limited, which means the product of their temporal width and their spectral width is a constant [34]:

$$\Delta E \Delta t = 0.44 \tag{5.6}$$

Where 0.44 is a numeric factor given for Gaussian pulses. The 50 fs pulses from the laser used for the measurements at the Ruhr University of Bochum have a spectral width of 19 nm, with a central wavelength of 800 nm. When such a pulse passes through a dispersive medium two things happen:

- The center of the pulse will arrive with a slight delay compared to a pulse travelling through air, this is called the group delay.
- They are elongated because the refractive index of the material is a function of wavelength. This elongation will also bring a chirp upon the pulse. Most materials used in optical setups introduce a positive frequency sweep, so the higher energetic photons are delayed more than the lower energetic ones.

The first point does not influence the autocorrelation measurement, because there are no dispersive materials, through which only one of the split beams has to pass. The second part however greatly affects the measurement of short pulses. Figure 5.3 shows how the dispersive broadening of a pulse is affected by its initial pulse length. It can be seen that for pulses longer than 100 fs the broadening in 10 mm of BK7 glass can be neglected, because the spectral width of the pulses then is so short, that they can be treated as monochromatic and hence are hardly affected by dispersion.

In order to calculate the effects of this dispersive broadening, one considers the phase shift φ as a function of frequency ω, $\varphi(\omega)$ can then be developed as a power series around ω_0, the center frequency [35]:

$$\varphi(\omega) = \varphi(\omega_0) + (\omega - \omega_0)\varphi'(\omega_0) + \frac{1}{2}(\omega - \omega_0)^2\varphi''(\omega_0) + \frac{1}{6}(\omega - \omega_0)^3\varphi'''(\omega_0) + ... \tag{5.7}$$

Whereas

$$\varphi'(\omega_0) = \left.\frac{\partial\varphi}{\partial\omega}\right|_{\omega=\omega_0},\ \varphi''(\omega_0) = \left.\frac{\partial^2\varphi}{\partial\omega^2}\right|_{\omega=\omega_0} \text{ and } \varphi'''(\omega_0) = \left.\frac{\partial^3\varphi}{\partial\omega^3}\right|_{\omega=\omega_0} \tag{5.8}$$

φ' is called the group delay, φ'' the group delay dispersion (GDD) and φ''' is the third-order dispersion (TOD).

For a Fourier transform-limited Gaussian pulse with a full width at half maximum pulse length of τ_{in} and a center frequency of ω_0 the electric field E_{in} has the following form:

$$E_{in}(t) = E_0 \exp\left[-\frac{2ln(2)\cdot t^2}{\tau_{in}^2} + i\omega_0 t\right] \tag{5.9}$$

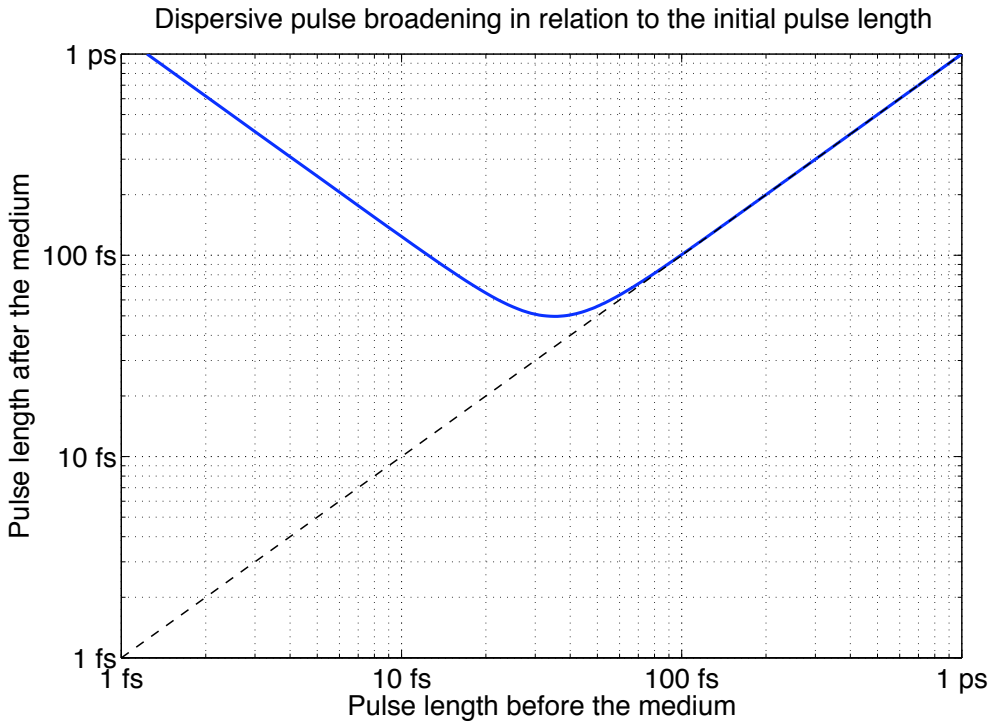

Figure 5.3: Calculated dispersive pulse broadening of a Fourier transform limited initial pulse that passes through 10 mm of BK7 glass.

To calculate the electric field after it has been propagating through a dispersive medium one needs to perform a Fourier transformation to write E_{in} in the frequency domain, then the components of the phase expansion $\varphi(\omega)$ from equation 5.7 have to be added before transforming the electric field back into the time domain.
If we assume that only the group delay dispersion (GDD) contributes and that the other terms can be neglected, then the electric field after the propagation through the medium can be written as:

$$E_{out} = E_0 \exp\left[i(\omega_0 t - \varphi) - \Gamma(t - \varphi')^2\right] \tag{5.10}$$

With

$$\Gamma = \left(\frac{\tau_{in}^2}{2ln2} + 2i\varphi''\right)^{-1} \tag{5.11}$$

By comparing equation 5.10 with equation 5.9, broadening and the frequency sweep can be seen. For the broadening the Gaussian part of E_{out} has to be investigated, then the new pulse length τ_{out} can be derived. The stretch factor can be written as:

$$\frac{\tau_{out}}{\tau_{in}} = \sqrt{1 + \frac{\varphi''^2}{\tau_{in}^4} 16(ln2)^2} \tag{5.12}$$

The frequency sweep can be seen by the fact that equation 5.11 is complex with a sign that is opposite to that of φ''.
In order to practically compute the broadening of the pulse, the group delay dispersion φ''

needs to be calculated. It is proportional to the length l_m of the material and the second derivative of the refractive index $n(\lambda)$:

$$\varphi''_m = \frac{\lambda_0^3 l_m}{2\pi c^2} \frac{d^2 n(\lambda)}{d\lambda^2} \tag{5.13}$$

Data for the refractive indices for optical materials was taken from [36]. It was assumed that $\tau_{in} = 50fs$ which fits the description in the data-sheet of the laser. A list of all dispersive materials and their thicknesses can be found in table 5.1. The acrylic glass block of 40.25 mm was used to elongate the pulses even more, to see the effects of dispersion very clearly. The autocorrelation traces recorded with and without the acrylic glass block for the GaAlAs LED and the GaAsP photodiode can be found in Figure 5.4. It was assumed that $\varphi''_{Total} = \varphi''_{57.24,BK7} + \varphi''_{2,FS} + \varphi''_{1.6,Quartz} + \varphi''_{40.25,AG}$. The dispersive materials were treated as if they all were directly behind each other and the air in between would not affect the beam.

This way, we get a stretch factor of 3.15 if the beam goes through all the dispersive materials apart from the acrylic glass block and a factor of 6.97 with the acrylic glass block. This results in pulse lengths of 157 ± 13 fs and 348 ± 33 fs. The errors come from the uncertainty in the pulse length of 50 fs which was assumed to be ± 5 fs, the effects of the other factors could be neglected because their uncertainties were significantly smaller and did not scale with the forth power.

The values for the experimentally derived pulse length which are depicted in Table 5.2 are significantly longer than the predicted pulse length which took the dispersion into account. A possible explanation for that is that the dispersion inside the detector might play a bigger role than expected. Similar measurements carried out by other groups with LEDs or photodiodes as detectors show similar results [21], [22]. For the measurement of ps-pulses this should however not play a significant role, since the pulse length is significantly longer and an accuracy of several hundred femtoseconds would be sufficient.

Optical component	Material	Thickness [mm]
Quartz-Retarder Zero order (RZQ2.10 for 810 nm from B.Halle)	Quartz (SiO_2)	1.6
Beam Cube Polarizer (TWK 1.10 from B.Halle)	Schott BK7	10
Neutral Density Filter (NDC-50C-2M from Thorlabs)	Fused Silica	2
780 nm Longpass-Filter (FGL780 from Thorlabs)	Schott RG780 treated as BK7	3
Beam Splitter (NT45-853 from Edmund Optics)	Schott BK7	4.24
Microscope Objective (25X)	assumed to be BK7	40
Acrylic glass block to elongate the pulses	Acrylic Glass	40.25
Total for Schott BK7		57.24
Total for Fused Silica		2
Total for Quartz		1.6
Total for Acrylic Glass		40.25

Table 5.1: The following dispersive components were placed along the beam path. The effects of the errors on the thickness of the materials was found to have a negligible effect on the pulse lengthening in comparison to the uncertainty of the initial pulse length itself, which was assumed to be 50 ± 5 fs

Detector	τ_{meas} without glass block	τ_{calc} due to dispersion	τ_{meas} with glass block	τ_{calc} due to extra-dispersion in block
Photodiode GaAsP	290 ± 1 fs	157 ± 13 fs	432 ± 2 fs	348 ± 33 fs
Red GaAlAs LED (2800 mcd)	391 ± 2 fs	157 ± 13 fs	521 ± 3 fs	348 ± 33 fs

Table 5.2: To elongate the pulses, the unsplit beam was sent through 40.25 mm of acrylic glass. τ_{meas} is the pulse length calculated with equation 5.3 from the fit parameters. The errors originate from the fit only. For τ_{calc} only the dispersive broadening of a 50 fs pulse going through the dispersive media listed in table 5.1 was taken into account. Dispersion inside the detector was neglected.

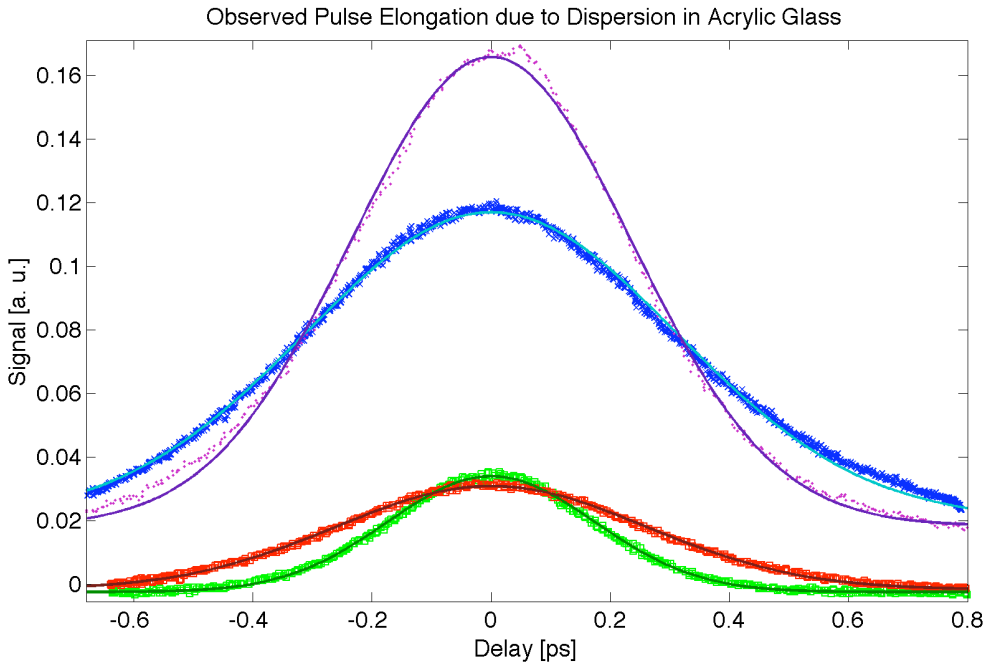

Figure 5.4: Autocorrelation signals recorded with a GaAsP Photodiode (green) and a GaAlAs LED (purple). Signal with a 40.25 mm thick acrylic glass block block for the GaAsP Photodiode (red) and the GaAlAs LED (purple). Also drawn are the Gaussian fits to the curves from which the pulse length was extracted. The optical power was measured to be 10 mW before the placement of the glass block. The signal of the LED was amplified by a factor of 40 more than that of the photodiode, however the ratio between the peaks is only 4.9. The signal of the photodiode is therefor around 8 times larger than that of the LED.

5.6 Autocorrelation Signals for Different Beam Intensities

In order to find the lower limit for the optical input power, the laser beam was attenuated further until no clear autocorrelation signal was visible any more. The attenuation was controlled with the neutral density filter and the beam cube polariser. The autocorrelation curves are illustrated in Figures 5.5 and 5.6. It is of interest to see not only how the peak signal depends on the optical input power, but also to investigate the effects on the measured pulse length in dependence of the optical input power.

5.6.1 Peak Signal Dependence on the Optical Input Power

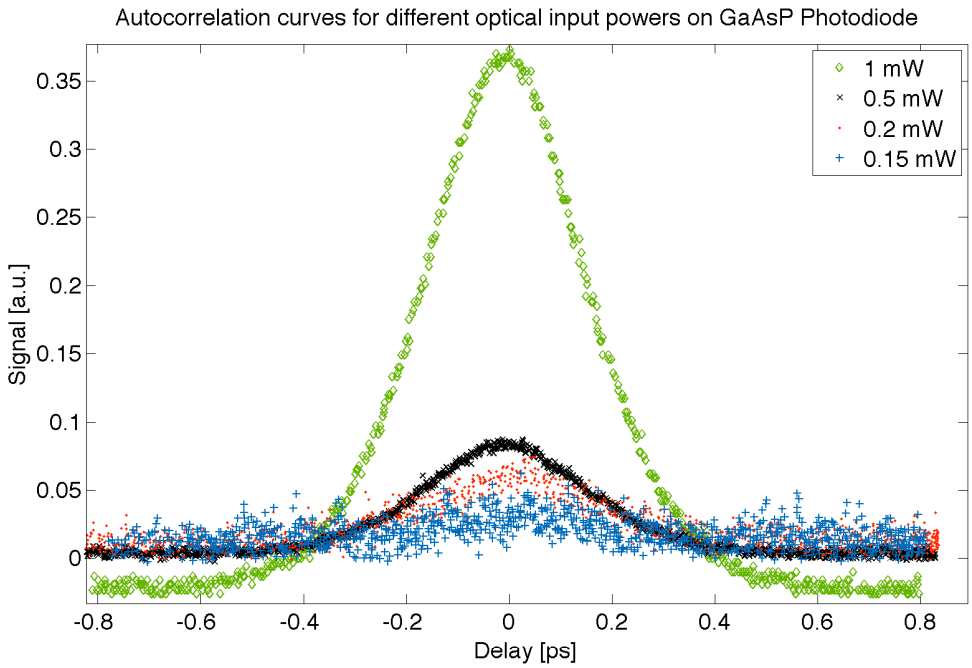

Figure 5.5: Autocorrelation signals recorded with a GaAsP photodiode. The curves were measured for different optical input powers. The optical input power was measured right before the beam went into the microscope objective to be focussed onto the detector. The measurement at 1 mW was taken with a smaller amplification factor on the current to voltage amplifier, hence the change of background level between the measurements.

In Figure 5.7 the fitted values for the peaks (after background subtraction) are plotted over the optical input power. The two sets recorded with the photodiode show how problematic the alignment is, for set 1 the alignment was a lot better than for set 2, so the signal is significantly larger, but the reproducibility is troublesome.

5.6.2 Pulse Length Dependence on the Optical Input Power

In order to obtain an estimate of the error of the pulse length measurement, the same data sets which have been investigated regarding their peak signal in the previous section have then been analysed regarding the initial laser pulse length they predict. This is depicted in Figure 5.8, the error bars are solely from the accuracy of the fits. It can be seen that

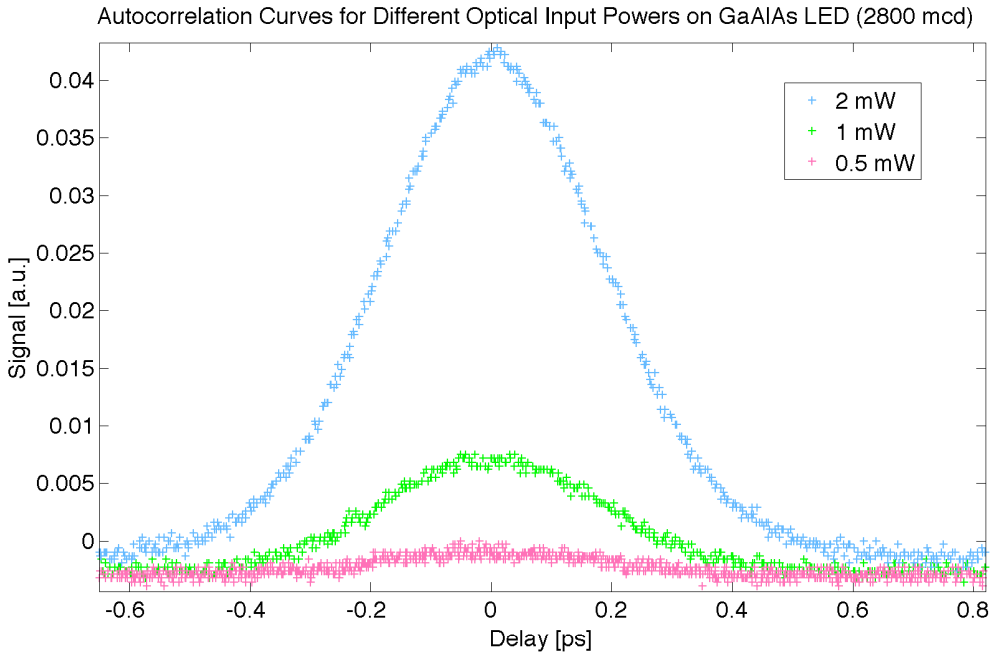

Figure 5.6: Autocorrelation signals recorded with a GaAlAs LED (2800 mcd), the curves were measured for different optical input powers. The optical input power was measured right before the beam went into the microscope objective to be focussed onto the detector.

for very low input powers all of the detectors predict shorter pulse length values than for higher optical powers. It is expected that the detector sees some kind of saturation for high optical input powers which leads to a broadening of the autocorrelation curve, this could already be seen for the measurements at 10 mW, for optical input powers below 0.5 mW the results vary greatly and also the errors of the fits become rather large. To make an assumption how precise the measurements are the difference between maximum and minimum values for the pulse length have been divided by two for the different detectors and are stated as the final errors on the measurement.

Detector	$P_{opt} \leq 1\,mW$	$P_{opt} \geq 1\,mW$
PD Set 1	265 ± 24 fs	265 ± 5 fs
PD Set 2	275 ± 41	287 ± 10
LED 2800 mcd	295 ± 62	310 ± 7

Table 5.3: Comparison of the measured pulse lengths and their errors for different detectors and different optical input powers. The central values are the weighted average values of the different data sets in the given optical power range.

The result of the pulse length obtained for the LED which are depicted in table 5.2 was considerably longer than the ones recorded during a different set, which is depicted in Figure 5.8 and Table 5.3. Unfortunately no further measurements with the LED during

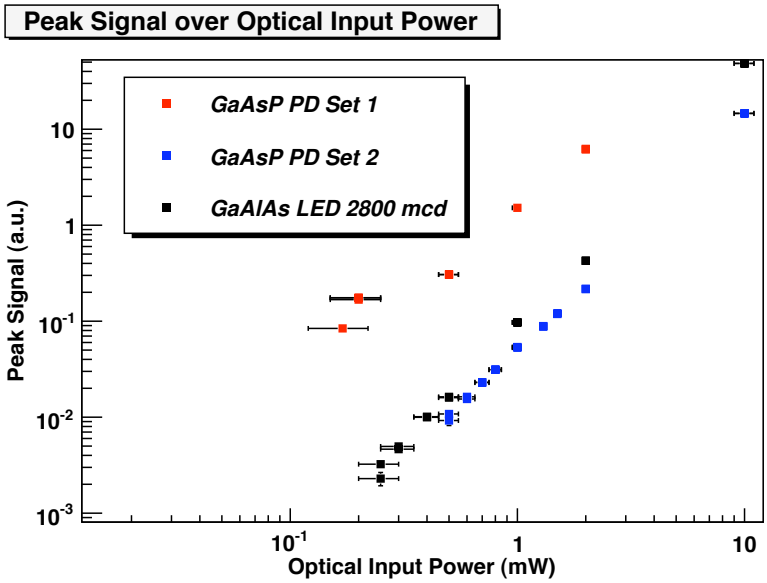

Figure 5.7: Value of the peak signal from the autocorrelation curves over optical power (the peak value is taken from the fit directly, the background level is ignored). Recorded with the GaAsP photodiode and the GaAlAs LED (2800mcd). The errors of the optical input power come from the resolution of the powermeters (for optical powers of more than 2 mW a different powermeter had to be used which had a rather poor resolution). The errors of the peak signal are taken from the Gaussian fits to the autocorrelation traces.

the set for which the pulse elongation in media was recorded, were measured. It is unclear where the significantly longer result originates from. One reason could be that the LED was not placed in the focus of the beam, which could have lead to a broadening due to a higher impact of the chromatic aberation.

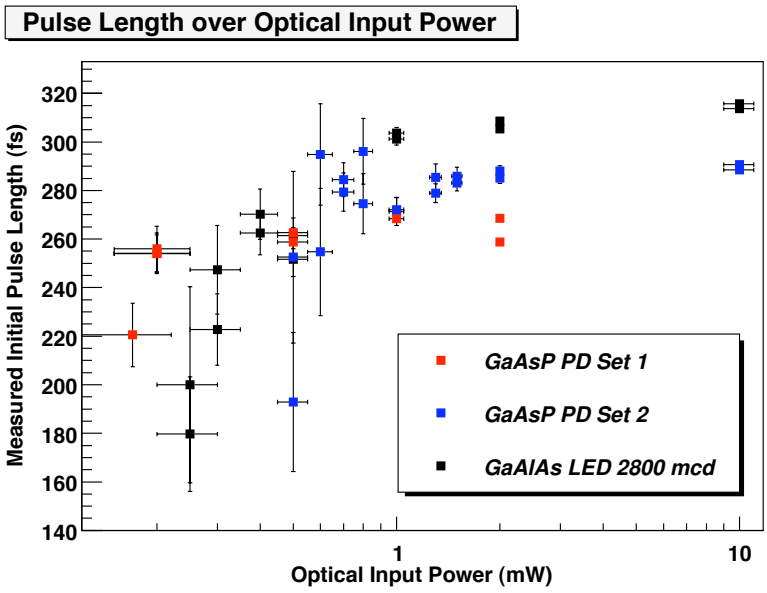

Figure 5.8: For this plot the measured initial pulse length (FWHM) τ_{meas}, which was obtained from the fits to the autocorrelation traces, is plotted over the optical input power. The different data sets are the same as in Figure 5.7. The vertical errors are taken from the fits, as previously. It can be seen that for all detectors the measured initial pulse length gets shorter at very low optical input powers and rises towards higher ones.

5.6.3 Using Profile Histograms to Reduce the Noise at Low Optical Input Powers

Especially at low optical input powers the noise of the amplifiers plays quite a significant role. In order to reduce this noise, autocorrelation traces were recorded over several periods of the delay scanner. The data was then put into a profile histogram with ROOT [32]. In Figure 5.9 an example of such a profile histogram is given. It can be seen that the noise mostly averages out nicely. For this measurement the data was recorded for roughly 30 minutes. This technique however does work a lot better with a laser source than with synchrotron light, because the beam current and henceforth the optical input power decreases with time for the synchrotron. Also, as explained in chapter 2.4, the bunch length and therefor also the optical pulse length is dependent on the bunch current, which makes long average times only possible for very stable conditions. Stable conditions are generally not reached while the beam current is very high.
In Figure 5.9 another effect can be seen: The shape of the autocorrelation trace seems to change for very low optical input powers. The Gaussian shape is altered into a more triangular looking shape. This behaviour has been noticed with the photodiode as well as with the LED when the optical power was just slightly above the resolution limit. A triangular autocorrelation trace could point towards a rectangular incidence pulse shape. It is, however, not expected that the pulse shape changes when the beam is attenuated. Furthermore this effect has been observed at different optical input powers for the photodiode and the LED. Most likely the effect is an artefact of the decreasing signal intensity.

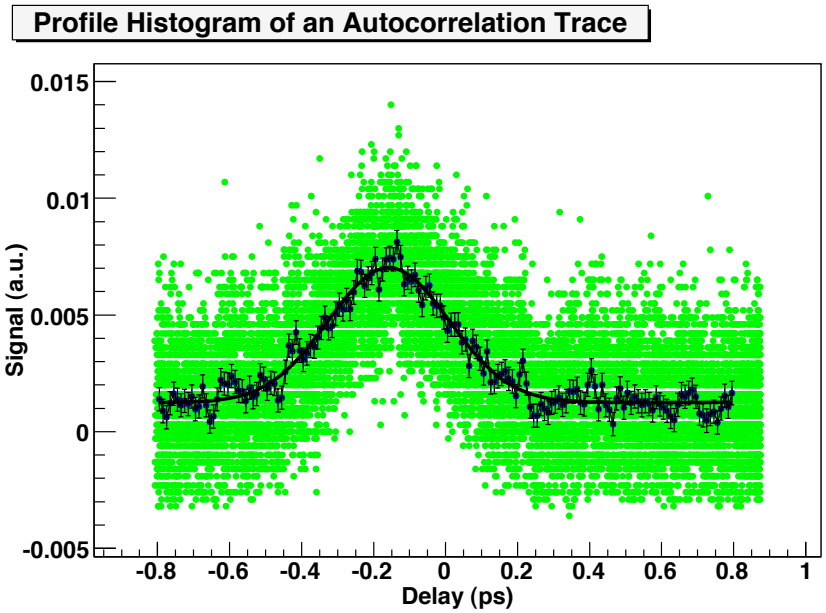

Figure 5.9: The raw data of the recorded autocorrelation trace (green) was put into a histogram with 160 bins between -0.8 and 0.8 and for each bin the average value is displayed (blue). The autocorrelation trace itself was recorded over many periods of the delay scanner to achieve enough data to average. Because the shape looks more triangular than Gaussian the FWHM of 0.32 ± 0.11 ps was taken directly from the data without a Gaussian fit. When applying a Gaussian fit the FWHM was found to be 0.39 ±0.1. The discrepancy comes mainly from the problem that the actual peak is not resembled very well by the Gaussian fit. The data was recorded for the GaAsP photodiode at an optical input power of 0.7 mW.

5.7 Measurements with Synchrotron Light

Even though the measurements with the synchrotron light did not yield the desired results, they brought along better knowledge of the characteristics of the radiation seen at the beamlines. The experimental results and theoretical predictions are discussed in the following sections of this chapter.

5.7.1 Validation of the Linear Increase in Radiation Power with the Beam Current

Equation 2.3, was experimentally validated. The results are shown in Figure 5.10. This measurement was executed to simplify the synchrotron measurements. Rather than measuring the optical power during the measurements, it was enough to measure the optical power at the start of a measurement for a known beam current. The beam current was logged in order to know at which optical power a measurement took place. This linearity, however, only holds well while the orbit remains unchanged. Changes in the beam position can lead to a slight increase or decrease of the intensity detected at the beamline. In order to take this into account, the beam position was logged as well.

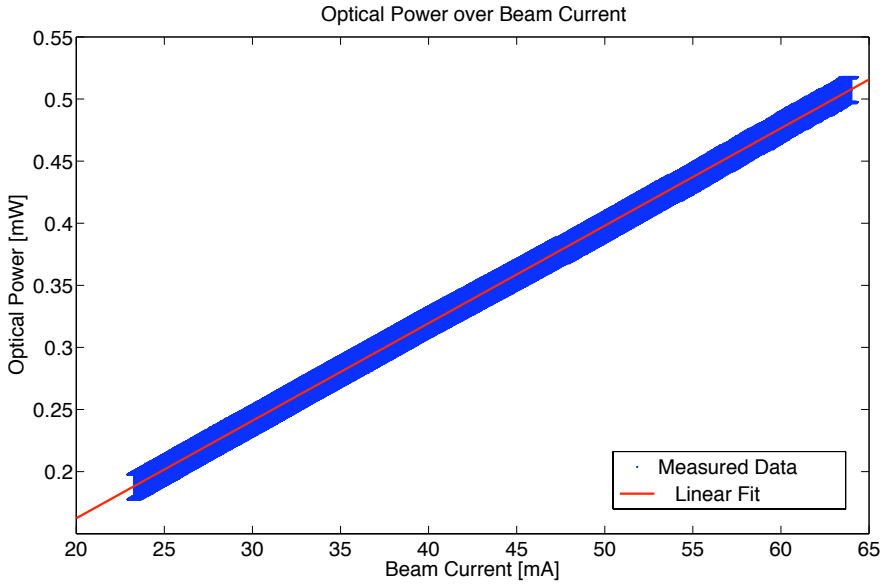

Figure 5.10: Experimental validation of the linear increase of the power of the synchrotron radiation (equation 2.3) with the beam current.

5.7.2 Beam Size, Focus & Intensity

At ANKA, there are two infrared beamlines present. The IR1 beamline and the IR2 beamline. The latter one is still in the commissioning phase and not available for users yet, its optical beam port could however be accessed to carry out measurements. The optical power was measured at both beamlines to determine where the intensity is higher. These measurements were undertaken during the normal user operation, so the beam energy was 2.5 GeV. The optical power was measured right behind the beam port window

with a power meter (PM-100 from Thorlabs). A 780 nm long-pass filter was applied. At the IR2 beamline an optical power of 1.8 mW could be measured at beam current of 94 mA, at the IR1 beamline a value of 0.5 mW was measured at a beam current of 93 mA. It is to mention that the power meter is only sensitive to wavelengths up to 1100 nm. This large difference (factor of 3.6) comes most likely from the fact that at the IR1 beamline there is a diamond window and a quartz window in use which are optimised for the IR wavelength range. At the IR2 beamline there is only one final window at every beam port. For the port at which this measurement took place, the material of the window is currently plain glass until it is upgraded when the beamline is fully commissioned. Because the autocorrelation set up requires a high intensity the measurements were carried out at the IR2 beamline, which we could kindly access during the commissioning phase.

The synchrotron radiation beam which leaves the optical beam port at the IR beamlines is not as small and evenly shaped as a conventional laser beam. This alone makes it harder to achieve a precise optical alignment. Another challenge is that the beam is not completely parallel. In order to compensate this a lens was placed near to the beam focus to generate a parallel beam (telescopic set up). A photograph taken of the beam at the IR1 beamline can be seen in figure 5.11.

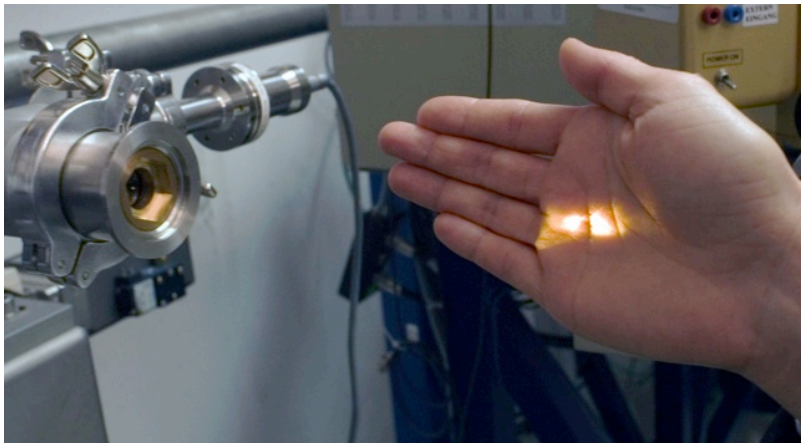

Figure 5.11: Picture of the visible synchrotron radiation beam at the IR1 beamline at ANKA. Courtesy of the IR Group.

5.7.3 Estimation of the Required Optical Input Power

The main goal of the laser measurements was to determine the lower intensity limit for which the autocorrelation trace could still be seen. In order to do this, comparing the average optical power is not enough, since the signal also depends on the peak power. It is common practice to use the product of peak power and average power to state the sensitivity of an autocorrelation set up [18]. In order to estimate the intensity needed from the synchrotron radiation depending on the lower limit that has been found experimentally with the laser measurements, the product of average power and peak power, $P_{avg} \cdot P_{peak}$, of the synchrotron has to be equal to the one of the laser at the lowest possible intensity that still allows to see an autocorrelation trace.

The power meter used for this (PM-100 from Thorlabs) can only measure the average optical power, it does so with a photodiode for which the current is calibrated. The peak power can be assumed if the repetition rate and the pulse length is known.

$$P_{peak} = \frac{P_{avg}}{f_{rep} \cdot \tau} \tag{5.14}$$

Whereas τ is the FWHM pulse length of the laser. With equation 5.14 the product can be written as follows:

$$P_{peak} \cdot P_{avg} = \frac{P_{avg}^2}{f_{rep} \cdot \tau} \tag{5.15}$$

The laser has a repetition rate of 1 GHz. For the synchrotron radiation the repetition rate depends on the filling pattern. The maximum possible value would be 500 MHz because this is the frequency of the RF cavities. It would mean that every one of the 184 RF buckets has to be filled, this however can lead to instabilities. During normal user operation and the low α_c-operation there are three bunch trains containing 33 bunches each. This leads to a total of 99 bunches every 368 ns (one circumference), which results in a repetition frequency of 269 MHz. For single bunch operation f_{rep} simply is the revolution frequency $f_{rev} = 2.7$ MHz.
We can now compare $P_{avg} \cdot P_{peak}$ for the laser and for the synchrotron radiation produced by ANKA:

$$\frac{P_{avg,min,Laser}}{f_{rep,Laser} \cdot \tau_{Laser}} : \frac{P_{avg,ANKA}^2}{f_{rep,ANKA} \cdot \tau_{ANKA}} = \frac{P_{avg,min,Laser}^2}{P_{avg,ANKA}^2} \cdot \frac{(f_{rep} \cdot \tau)_{ANKA}}{(f_{rep} \cdot \tau)_{Laser}} \stackrel{!}{=} 1 \tag{5.16}$$

In order to be able to compare the signal with the synchrotron light with the one of the laser, equation 5.16 must equal one. We have shown in Figure 5.5 that the lower limit of the optical input power for the GaAsP photodiode lies around $P_{avg} = 0.15$ mW measured with the chopper running right before the microscope objective in the experimental set up. For the pulse length of the laser, the value that can be extracted from the autocorrelation curve is taken without any corrections, because this is the pulse length that reaches the detector. So $\tau_{Laser} \approx 290\,fs$, which results in:

$$\frac{P_{avg,min,Laser}}{f_{rep,Laser} \cdot \tau_{Laser}} = 77.6(mW)^2 \tag{5.17}$$

If we now put equation 5.17 in equation 5.16 and rearrange it we get the following:

$$P_{avg,ANKA} = \sqrt{112.5(mW)^2 \cdot (f_{rep} \cdot \tau)_{ANKA}} \tag{5.18}$$

For the normal user operation with $\tau = 70\,ps$ and $f_{rep} = 269\,\mathrm{MHz}$ we get:

$$P_{avg,ANKA} = 1.2\,\mathrm{mW} \tag{5.19}$$

For the low α_c operation with strong bunch length reduction, that generates a stable beam, we have $\tau = 9\,ps$ (lowest value measured with Streak Camera) and $f_{rep} = 269\,\mathrm{MHz}$ we obtain:

$$P_{avg,ANKA} = 430\,\mu W \tag{5.20}$$

For the low α_c single bunch operation with the same bunch length reduction we have $\tau = 9\,ps$ as well but $f_{rep} = 2.7\,\mathrm{MHz}$ we get:

$$P_{avg,ANKA} = 43\,\mu W \tag{5.21}$$

In equation 2.3 it was shown that the average optical power of ANKA is directly proportional to the current stored in the ring. This current can then be expressed as the average bunch current times the number of bunches:

$$P_{avg}(ANKA) \sim I_{\mathrm{beam}} \sim I_{\mathrm{bunch,\ avg}} \cdot \#\ \mathrm{Bunches} \tag{5.22}$$

For the infrared range of the spectrum the proportionality factor between P_{avg} and I_{beam} is nearly independent of the beam energy. We learn from equations 5.21 and 5.20 that a single bunch measurement is only worthwhile if we can increase the bunch current by a factor of 10 compared to the normal bunch current we have during multi-bunch operation. At the moment we reach a bunch current of around $I_{bunch,multi} \approx 1.5$ mA for multi-bunch operation and $I_{bunch,single} \approx 3$ mA. Furthermore it should be noted that during the normal user operation with 2.5 GeV, the beam current is around $I_{beam} \approx 150$ mA, for the low α_c operation at 1.3 GeV the beam current at the fully squeezed state is only about 75 mA, so the optical power is two times lower. When comparing equations 5.19 and 5.20 one sees that during the fully squeezed low α_c operation the signal should be highest, so this was picked for a measurement. Unfortunately the optical power reached at the optical beam port at the IR2 beamline at ANKA after the application of the 780 nm longpass filter and with the chopper running (same settings as for the power measurement with the laser) was only 220 μW.

If we calculate at which optical power of the laser a signal should still be obtained, we get a value of 75 μW from eqation 5.16, which is only a factor of two lower than what was present on the measurement with 150 μW. This gave the motivation to attempt another measurement with the synchrotron radiation. Some of the recorded data is depicted in Figure 5.13.

5.7.4 Expected Influence due to Dispersion

In this section, the possible influence of dispersion effects on the determination of the synchrotron radiation pulse length is discussed.

There are two main differences between the synchrotron radiation and the radiation produced by the fs-laser used for previous measurements:

- The pulse length of the synchrotron pulses is considerably longer (FWHM ≈ 3 - 70 ps).
- The radiation is not Fourier transform limited.

In general synchrotron radiation has a very wide spectrum ranging from the far infrared (FIR) via the visible into the X-ray range (see chapter 2.3), however the actual spectrum at the beam port of a beamline depends highly upon the design of the beamline. At

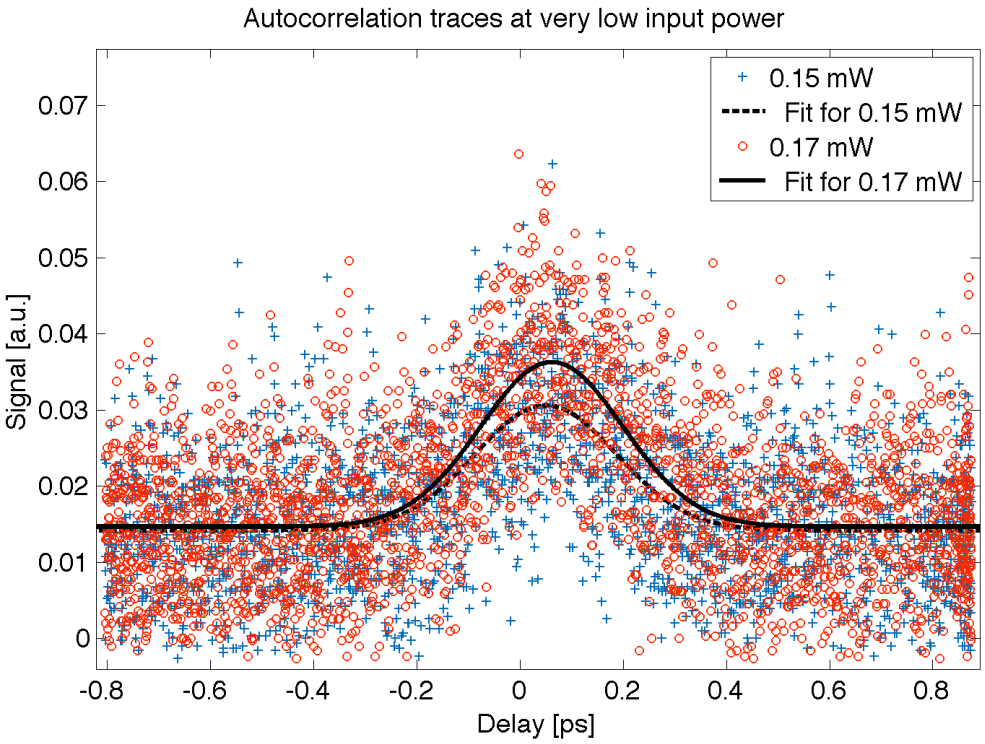

Figure 5.12: Autocorrelation traces recorded with a GaAsP photodiode (G1118) for a Gigaoptics fs-laser at the Ruhr University of Bochum. The traces have been recorded at very low input power and the amplification of the signal was set to the maximum possible values.

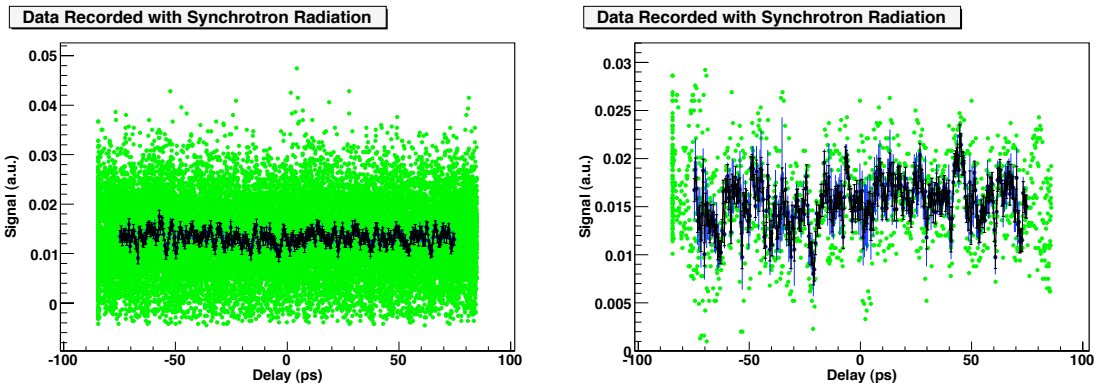

Figure 5.13: Data recorded with the synchrotron radiation. Left: Averaged over a long time scale to obtain sufficient statistics. The beam was fully squeezed at 1.3 GeV, with a current of around 62 mA. The optical power was measured to be only around 50 μW. Right: Data recorded over a shorter time. The beam current was 173 mA at 1.3 GeV (unsqueezed) and the optical power was measured to be around 200 μW.

an infrared beamline, for example, X-rays are not desired, so they are filtered out. My measurements were undertaken at an IR beamline, where a combination of gold mirrors and a diamond window is used to filter out all the undesired wavelengths. For the autocorrelation experiment a 780 nm long pass filter had to be used to filter out photons

which have enough energy to cross the bandgap in the semi-conductor used as detector, so the photons present for the experiment ranged between 780 nm and several micrometers. The beamsplitter used (NT45-853 from Edmund Optics) has a special kind of NIR coating that is designed for wavelengths between 700 nm and 1100 nm. For longer wavelengths more radiation gets reflected than transmitted, leading to an overall decrease of intensity for those wavelengths because the photons reaching the detector are reflected once and transmitted once by the beam splitter.

The influence of dispersive media on the synchrotron light pulses can be estimated in the following way: For the set up with the synchrotron radiation no retarders were needed. The only dispersive media the beam had to pass through were a lens, the beam splitter and the microscope objective, all made out of Schott BK7 glass. Their total thickness is roughly 48 mm. If we assume that the main contribution comes from photons between 800 nm and 1100 nm, the difference in runtime for a photon of 800 nm and one of 1100 nm going through 48 mm of Schott BK7 glass can be calculated as follows:

$$\Delta t = \frac{\Delta x \cdot \Delta n_{800nm/1.1\mu m}}{c} = \frac{48mm \cdot (1.51078 - 1.50617)}{c} = 0.74\,ps \tag{5.23}$$

The data for the refractive indices was taken from [36], as previously. So when measuring during the low α_c operation, the dispersion has to be taken into account. For the longer pulses generated during the normal user operation the effects of dispersion are not so significant. For comparison Δt has also been calculated for the pulses passing through 1 m of air, where the runtime difference is only about 4 fs, so this can be neglected for synchrotron measurements.

6. Streak Camera Measurements

In the framework of this work, various streak camera measurements were carried out to obtain a better understanding of the streak camera and its possibilities along with its limitations. The basic working principle of the streak camera has already been pointed out in chapter 3.2, along with the problem of averaging which is required to obtain a sufficiently bright image.
Several improvements to the set up and the analysis of the data were carried out, such as applying a band pass filter to decrease the effects of dispersion and slightly altering the set up to focus the radiation onto the detector. Coherent oscillations (e.g. the synchrotron frequency) were taken into account in the offline analysis of the image data to reduce the smearing out in a long term average. When finally the single bunch operation became available a lot of new possibilities to obtain a better resolution of the pulse length opened up. Several single bunch measurements have been undertaken to measure not only the pulse length but also the pulse profile.

6.1 Analysis of the Streak Camera Images

The sweeping units of the streak camera are synched with the RF frequency divided by two and a fraction of the revolution frequency.
The sine wave of the RF frequency divided by two, which controls the fast sweeping unit, allows us to depict the light pulses from bunches coming from odd RF buckets at a different location on the screen than from the ones generated by bunches in even RF buckets. This however means that we do not know exactly where the head and the tail of the bunches lie, because they will have a different orientation depending on the delay time. If the time profile of a pulse is to be observed it is of great interest to see where the head and tail of a bunch lies, so this had to be determined. In order to do so the delay time was increased and it was observed whether the bunches move closer on the y-axis or further apart. This is illustrated in Figure 6.1.

In Figure 6.2 it is shown how the time axes are in relation to the pixel axes, which is important to know, since pixels are used as scale for the evaluation.

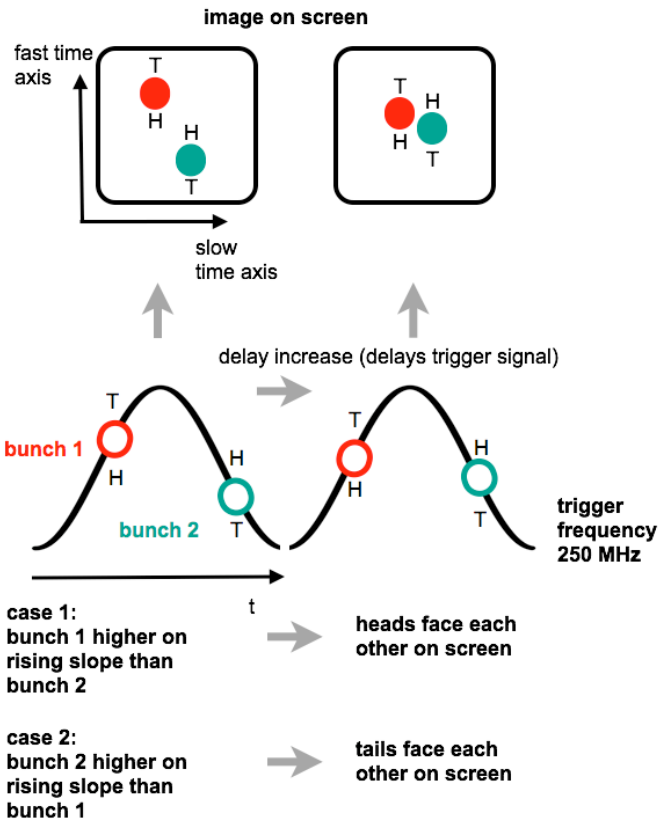

Figure 6.1: This figure illustrates how the orientation of the pulses depicted on the streak camera screen can be be determined by increasing the delay time of the trigger signal and then observing in which direction the bunches move along the vertical axis. Case 1 has been drawn, where bunch 1 is higher on the rising slope than bunch 2. T stands for tail and H for head, when looking at a time profile the head comes first and then the tail at a later time.

The revolution frequency, which is needed to trigger the slow time axis, is obtained by dividing the RF frequency by the harmonic number (h=184 for ANKA $\rightarrow f_{rev} \approx 2.7MHz$). Taking a picture of the fluorescent screen takes a few milliseconds because of the exposure time needed for the camera to produce a good quality picture, so the time between two consecutively recorded single streak camera images is at least several milliseconds depending on the exact exposure time. This is why the revolution frequency trigger signal has to be further divided to a signal with several Hz, which has to be phase stable to the revolution frequency. Jitter on any of those trigger signals further limits the resolution of the streak camera.

The effect of the time of arrival variation caused by the synchrotron oscillation can be seen with the streak camera (Figures 6.3 and 6.2 show examples of the oscillation), to allow an evaluation of the data, this rather stable oscillation can be subtracted from the data.

The evaluation is as follows: A consecutive sequence of single shot images is recorded. The data for every image is then binned along the x-axis (slow time) for every bin the projection onto the y-axis is performed and the average value is subtracted from all the values within that bin. This is performed for all bins in one image to get rid of the oscilla-

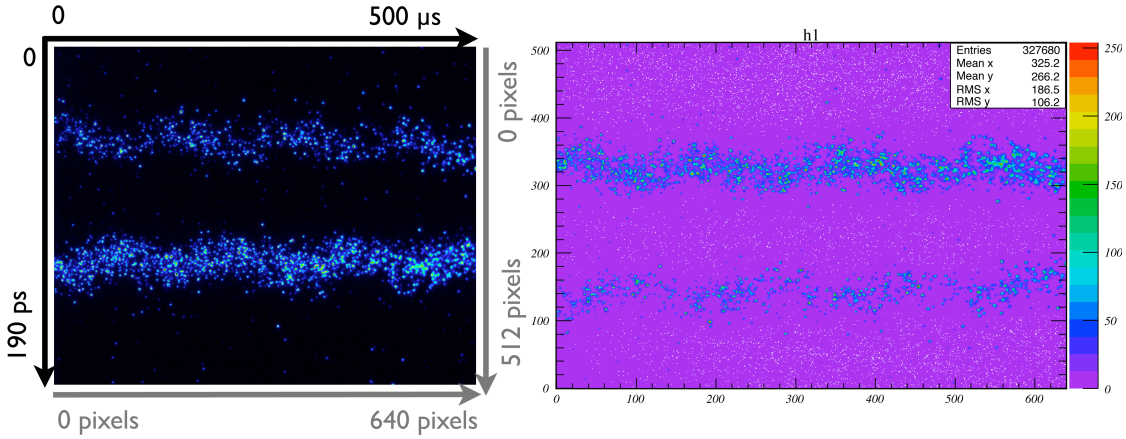

Figure 6.2: Left: This picture was recorded with the streak camera at ANKA. It shows the pulses coming from bunches in the odd RF-buckets separated from bunches in the even RF-buckets along the y-axis. The black axes are given by the streak camera software (supplied by Hamamatsu), when the picture is exported only a pixel axis is given, for which the y-orientation runs the other way. Right: The same image imported into ROOT [32] with pixel axes.

tion. Then the projection onto the y-axis is performed. This is done for all images in the sequence (usually around 500) and the projections are summed up and a Gaussian fit is applied. In Figure 6.3 a single image from such a sequence is depicted and the results of the analysis for all images of the sequence is shown in Figure 6.4. The difference between the pulse length determined with the analysis of the streak camera data and the electron bunch length resulting from the measured synchrotron tune is more than a factor of two ($10 \pm 1ps$ from the tune and 25 ps from the streak camera), which could be explained by a current-depending bunch lengthening. In order to prove this assumption, further measurements were undertaken and are presented in the next section.

6.2 Observation of a Bunch Lengthening in Dependence of the Bunch Current

Because a bunch lengthening effect in dependence of the current is expected to be due to a CSR wake-field [12], measurements with the streak camera were undertaken during low α_c-operation. For a synchrotron frequency of 18.8 kHz at 1.3 GeV during single bunch operation several sequences of 500 pictures each were recorded at different bunch currents.

In Figure 6.5 the measurement series of the pulse length in dependence of the bunch current can be seen. The recorded data does exhibit the same behaviour which was recorded at BESSY II [12]. It can also be seen that the pulse length predicted from the synchrotron tune seems to represent the pulse length measured at very low beam currents very well. More measurements to record more data for different synchrotron tunes are planned and will be carried out over the next few months to obtain a better understanding of the bunch

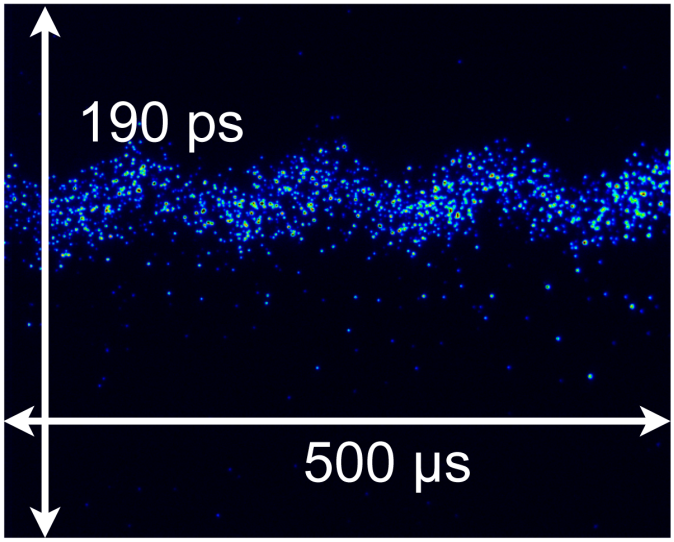

Figure 6.3: One streak camera image of a sequence consisting of 500 consecutive images recorded with the streak camera at ANKA. The oscillation is caused by the synchrotron oscillation of the electrons within the synchrotron. The image was taken during single bunch operation.

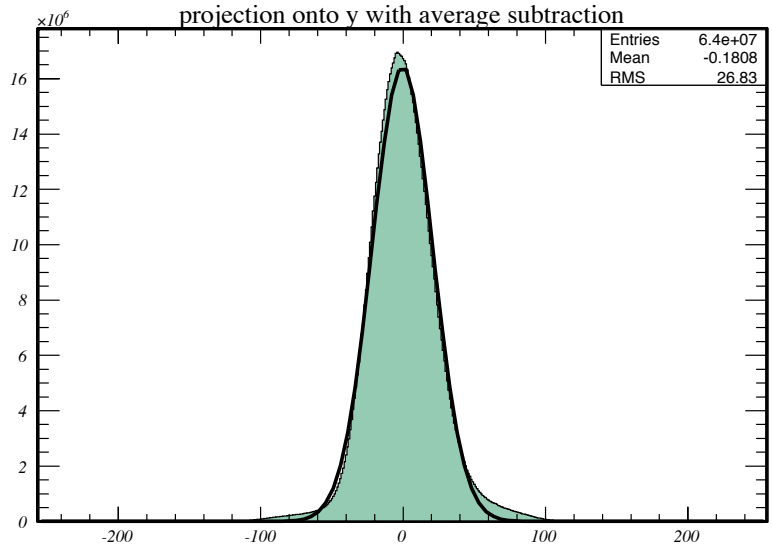

Figure 6.4: A summed up projection of all 500 images from the sequence depicted in Figure 6.3 with previous average subtraction. Fitted with a Gaussian distribution, the RMS value given in the graph is not in ps but in pixels, which can be translated to a FWHM value for the pulse length of 25 ps. The electrons inside the storage ring had an energy of 1.3 GeV and the RF voltage was set to 150 kV (in every cavity), the synchrotron frequency f_s was 7.2 kHz and the expected bunch length (FWHM) from this value is $10 \pm 1ps$.

lengthening and allow us to make better predictions of the pulse length based on the beam current and the synchrotron tune.

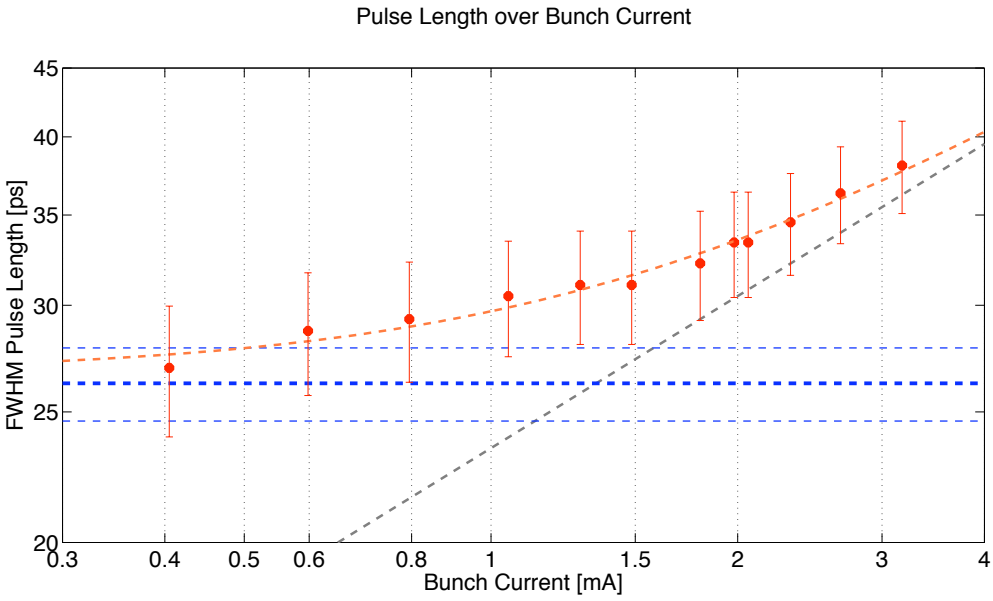

Figure 6.5: This figure shows the bunch lengthening in dependence of the beam current. In red is the data measured with the streak camera. The orange dotted line is a fit to the data to guide the eye. For the fit the following function was used: $(\frac{\sigma_z}{p_1})^4 = (\frac{f_s}{p_2})^4 + (\frac{I_b}{p_3})^{3/2}$ as it was done for the data recorded at BESSY II [12], here σ_z is the RMS pulse length and p1, p2 and p3 are fit parameters. The grey dotted line resembles the bursting stable threshold and the blue line is the prediction of the bunch length from the synchrotron tune with its prediction bounds. The error on the pulse length was taken to be $\pm$ 3 ps, which is a conservative estimation.

6.3 Observation of a Current-Dependent Bunch Deformation

It is expected that the bunch shape becomes deformed for higher currents [8]. In order to investigate this the pulse profiles for different beam currents were analysed.
In Figure 6.6 the pulse profiles were normalised to have the same area for every bunch current to picture the deformation with a steeper head and a slightly longer tail. In Figure 6.7 the same profiles are depicted but this time they are scaled with the bunch current. The observed deformation complies with the theory predicting that the head of the bunch becomes steeper and the tail becomes longer.

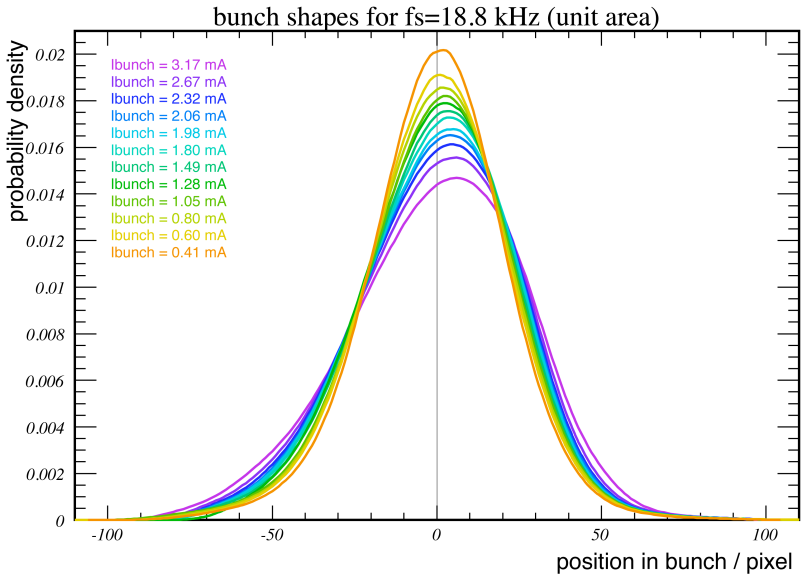

Figure 6.6: This figure shows the shape of the bunch recorded with the streak camera at ANKA at a synchrotron frequency of 18.8 kHz at 1.3 GeV during single bunch operation. All the curves are normalised to have the same area. It can clearly be seen that the pulses are deformed for higher bunch currents and exhibit a rather Gaussian shape for low bunch currents. The head of the pulse lies to the right.

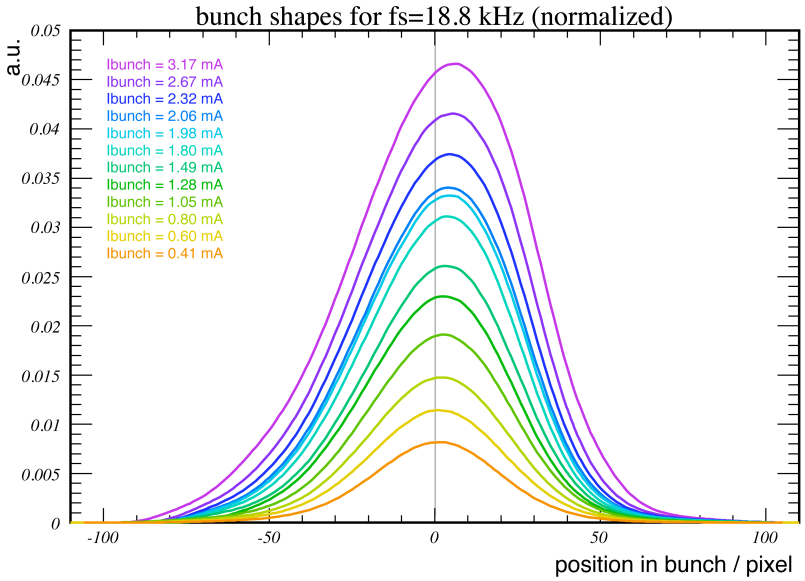

Figure 6.7: This figure shows the shape of the bunch recorded with the streak camera at ANKA at a synchrotron frequency of 18.8 kHz at 1.3 GeV during single bunch operation. The curves are normalised, but scaled with the bunch current. It can clearly be seen that the pulses are deformed for higher bunch currents and exhibit a rather Gaussian shape for low bunch currents. The head of the pulse lies to the right.

7. Conclusion

The bunch length along with the beam energy are important parameters of every synchrotron light source. The beam energy determines how short the wavelength of the emitted synchrotron radiation can be. The bunch length determines the length of the synchrotron radiation pulses, which is responsible for the resolution that can be achieved with time resolved measurements. The bunch length is also the main parameter for the creation of coherent synchrotron radiation (CSR).
The methods used up to now to determine the bunch length at ANKA all show different systematic effects which makes an interpretation of the results difficult. An independent method could therefor help to understand the various effects influencing the bunch length. In the framework of this thesis, a basic low cost intensity autocorrelation set up with a semiconductor detector to measure the synchrotron pulse length independently is presented. This method is commonly used to measure the pulse length of pulsed lasers, but has not yet been used to measure the length of synchrotron light pulses. Important improvements to the basic set up were needed to increase its sensitivity. This allowed to measure the pulse length of a fs-laser even at a very low optical input power of only 150 μW. The signal to background ratio could be increased from 3:1 to 18:1 at an optical power of 10 mW. This could be achieved by chopping the delayed and the undelayed beam at different frequencies and using a lock-in amplifier to filter out the undesired background. The characteristics of an LED and a photodiode as detector were compared. The photodiode was found to be more sensitive and easier to handle because of the larger chip size. The experimental outcome and theoretical estimations prove that the intensity of the emitted synchrotron radiation is just below the detection limit. The results did not allow an extraction of the pulse length from the recorded autocorrelation traces. A more advanced set up with a more sensitive detector (e.g. a photomultiplier tube) could be used for future experiments. This, however, would require a slightly different set up and photomultiplier tubes are more delicate to handle.

Recently the ANKA injector was upgraded with a new electron source that allows single bunch injection. The availability of single bunch operation allowed further studies of the

characteristics of the streak camera, one of the devices used at the ANKA storage ring to determine the pulse length. Modifications of the the streak camera set up and to the settings within the control software were undertaken to improve the image quality and resolution. The analysis of the recorded data was optimised. The optimised experimental conditions allowed for the first time a clear measurement of the current dependence of the pulse length and pulse shape in the low α_c-mode.

Acknowledgements

First of all, I would like to thank the professors Baumbach and Quast for allowing me to write this thesis. Special thanks also go to Anke-Susanne Müller, my supervisor, for her strong commitment. She encouraged me when needed and did not despair when I asked countless questions. Furthermore I want to thank Anton Plech who did not only lend me a lot of his optical equipment and helped me to set up a first test measurement with his fs-laser, but also taught me a lot about what to take into consideration when building an optical set up. Further thanks go to Erik Bründermann whose idea it was to see whether an intensity autocorrelation works with synchrotron radiation or not. He also supplied me with the ScanDelay unit, an alignment laser and made it possible that I could do test measurements at the Ruhr University of Bochum. Many thanks go to his PhD student Matthias Krüger, who helped me to carry out my experiments in Bochum and improved the LabView program to read out the data. Thanks also go to Erhard Huttel for operating ANKA during most of my beam time shifts. Another person who needs to be mentioned here is Nigel Smale who helped me to understand the electronics behind my set up and supplied me with all sorts of bits and pieces lying around in his "magic box". Of course, special thanks go to all the members of the THz-group, who have been very helpful in all aspects, especially Vitali Judin who assisted me during the long measurement times and who programmed a basic LabView program to log the beam parameters along with the signal from a detector. Sebastian Marsching who helped me with all sorts of computer problems. To Steffen Hillenbrand, for encountering every LaTeX problem a little earlier than me, so he always had a solution ready. To Marit, who helped me with countless little things. Also Roland Bless, the author of the LaTeX template which I used as basis, deserves my thanks. The team of the infrared group, especially Yves-Laurent Mathis and Michael Süpfle deserve a big thank you, because they let me use their beamlines and supported me wherever possible. Thanks also go to the ANKA workshop team which is lead by Daniel Ritz, who helped me to prepare my detector and built a little mount for the ScanDelay. Furthermore I want to thank Udo Geckle and Michael Bruns from the IMT who coated the prisms with a thin layer of gold which I needed for a test set up. To Pedro Fernandes Tavares, Bastian Beskers and Bernhard Döring, who more or less volunteered to proof-read my thesis and gave me a lot of constructive feedback. Thanks also go to my boyfriend Stefan Ernst for the countless times he motivated and encouraged me and even helped me with some measurements and suggested changes to the style of this work. I would also like to thank my parents and my sister, who supported me throughout my

whole studies without ever fully grasping what I actually do (they were impressed by the looks of ANKA, though).

References

[1] C. Settakorn, M. Hernandez, and H. Wiedemann. Sub-picosecond electron bunch length measurement. In *Particle Accelerator Conference, 1997. Proceedings of the 1997*, volume 2, pages 2017–2019 vol.2, May 1997.

[2] Hung-chi Lihn, Pamela Kung, Chitrlada Settakorn, Helmut Wiedemann, and David Bocek. Measurement of subpicosecond electron pulses. *Phys. Rev. E*, 53(6):6413–6418, Jun 1996.

[3] Schmüser P. Walter G.v. Geitz M., Schmidt G. Sub-picosecond bunch length measurement at the TESLA test facility. *Nuclear Instruments and Methods in Physics Research Section A: Accelerators, Spectrometers, Detectors and Associated Equipment*, 445:343–347(5), 1 May 2000.

[4] T Mitsuhashi and M Tadano. Measurement of Bunch Length using Intensity Interferometry. In *Prodeedings of EPAC*, 2002.

[5] K. Wille. *Physik der Teilchenbeschleuniger und Synchrotronstrahlungsquellen.* Teubner Studienbücher, 1992.

[6] H. Wiedemann. *Particle Accelerator Physics I.* Springer, 1999.

[7] H. Wiedemann. *Particle Accelerator Physics II.* Springer, 1999.

[8] Marit Klein. *Untersuchung der Stupakov-Schwelle zur Erzeugung stabiler kohärenter Synchrotronstrahlung.* Laboratorium für Applikationen der Synchrotronstrahlung der Universität Karlsruhe, 2008.

[9] XOP (X-ray Oriented Programs) is a widget-based driver program that is used as a common front-end interface for computer codes of interest to the synchrotron radiation community. http://www.esrf.eu/UsersAndScience/Experiments/TBS/SciSoft/xop2.3/.

[10] F. Zimmermann M. G. Minty. *Measurement and Control of Charged Particle Beams.* Springer, 2003.

[11] Qin Q et al. Studies on the Beam Current Dependent Phenomena in the BEPC-II Storage Rings. *Proceedings of EPAC08, Genova, Italy, WEPC060*, pages 2130–2132, 2008.

[12] C. Biscari and W. Chou, editors. *Beam Dynamics Newsletter No. 35.* ICFA - International Committee for Future Accelerators, 2004.

[13] A.-S. Müller, I. Birkel, B. Gasharova, E. Huttel, R. Kubat, Y.-L. Mathis, D.A. Moss, W. Mexner, R. Rossmanith, M. Wuensch, P. Wesolowski, F. Perez, M. Pont, and C.J. Hirschmugl. Far Infrared Coherent Synchrotron Edge Radiation at ANKA. In *Particle Accelerator Conference, 2005. PAC 2005. Proceedings of the*, pages 2518–2520, May 2005.

[14] Anke-Susanne Müller. Physik der Teilchenbeschleuniger und Synchrotronstrahlungsquellen; Vorlesung, Universität Karlsruhe, 2007.

[15] Hamamatsu Photonics. Guide to Streak Cameras.

[16] Max-Planck Gesellschaft. *Schematic drawing of the principle of function of a streak camera.* http://www.mpg.de/bilderBerichteDokumente/multimedial/bilderWissenschaft/2004/02/Krausze2/pressebild.html.

[17] A.-S. Müller, S. Casalbuoni, M. Fitterer, E. Huttel, Y.-L. Mathis, and M. T. Schmelling. Modeling the Shape of Coherent THz Pulses Emitted by Short Bunches in an Electron Storage Ring. In *Particle Accelerator Conference, 2008. PAC 2008. Proceedings of the*, page 3 p, 2008.

[18] D.T. Reid, W. Sibbett, J.M. Dudley, L.P. Barry, B. Thomsen, and J.D. Harvey. Commercial Semiconductor Devices for Two Photon Absorption Autocorrelation of Ultrashort Light Pulses. *Appl. Opt.*, 37(34):8142–8144, 1998.

[19] Frank Träger, editor. *Handbook of Lasers and Optics.* Springer, 2007.

[20] A. Baltuska M. S. Pshenichnikov J. K. Ranka, A. L. Gaeta and D. A. Wiersma. Autocorrelation measurement of 6-fs pulses based on the two-photon-induced photocurrent in a GaAsP photodiode. *Optics Letters*, 22(17):1344–1346, September 1 1997.

[21] Syed Abdullah Aljunid. Optical Autocorrelation using Non-Linearity in a Simple Photodiode. Master's thesis, Department of Physics, National University of Singapore, 2006 / 2007.

[22] D. T. Reid, M. Padgett, C. McGowan, W. E. Sleat, and W. Sibbett. Light-Emitting Diodes as Measurement Devices for Femtosecond Laser Pulses. *Opt. Lett.*, 22(4):233–235, 1997.

[23] Toshiaki Hattori, Yoshitsugu Kawashima, Masahiro Daikoku, Hideyuki Inouye, and Hiroki Nakatsuka. Autocorrelation Measurement of Femtosecond Optical Pulses Based on Two-Photon Photoemission in a Photomultiplier Tube. *Japanese Journal of Applied Physics*, 39(Part 2, No. 8A):L809–L811, 2000.

[24] T. Krug, M. Lynch, A.L. Bradley, J.F. Donegan, L.P. Barry, H. Folliot, J.S. Roberts, and G. Hill. High-Sensitivity Two-Photon Absorption Microcavity Autocorrelator. *Photonics Technology Letters, IEEE*, 16(6):1543–1545, June 2004.

[25] H. Y. Cui, Z. F. Li, Z. L. Liu, C. Wang, X. S. Chen, X. N. Hu, Z. H. Ye, and W. Lu. Modulation of the two-photon absorption by electric fields in HgCdTe photodiode. *Applied Physics Letters*, 92(2):021128, 2008.

[26] F.R. Laughton, J.H. Marsh, and A.H. Kean. Very sensitive two-photon absorption GaAs/AlGaAs waveguide detector for an autocorrelator. *Electronics Letters*, 28(17):1663–1665, Aug. 1992.

[27] K. Kikuchi. Highly sensitive interferometric autocorrelator using Si avalanche photodiode as two-photon absorber. *Electronics Letters*, 34(1):123–125, Jan 1998.

[28] S.-D. Yang, A.M. Weiner, K.R. Parameswaran, and M.M. Fejer. 400-photon-per-pulse ultrashort pulse autocorrelation measurement with aperiodically poled lithium niobate waveguides at 1.55 μm. In *Lasers and Electro-Optics, 2004. (CLEO). Conference on*, volume 1, pages 2 pp. vol.1–, May 2004.

[29] F.R. Laughton, J.H. Marsh, D.A. Barrow, and E.L. Portnoi. The two-photon absorption semiconductor waveguide autocorrelator . *Quantum Electronics, IEEE Journal of*, 30(3):838–845, Mar 1994.

[30] On loan from Erik Bründermann from the Institute of Physical Chemistry II of the Ruhr University of Bochum.

[31] Simon Ebbinghaus. *Aufbau eines THz-Femtosekundenspektrometers zur zeitaufgelösten Spektroskopie von Proteinen in Flüssigkeiten.* Ruhr-Universität Bochum, Fakultät für Chemie, Physikalische Chemie II, Prof. Havenith, 2004.

[32] ROOT is a system that provides a set of frameworks with all the functionality needed to handle and analyze large amounts of data in a very efficient way. http://root.cern.ch/drupal/.

[33] K. Taira, Y Fukuchi, R. Ohta, K. Katoh, and K. Kikuchi. Background-free intensity autocorrelator employing si avalanche photodiode as two-photon absorber. *Electronics Letters*, 38(23):1465–1466, Nov. 2002.

[34] Rudiger Paschotta. Encyclopedia of laser physics and technology, 2006.

[35] Gavin D. Reid and Klaas Wynne. Ultrafast Laser Technology and Spectroscopy. *Encyclopedia of Analytical Chemistry*, pages 13644–13670, 2000.

[36] http://refraciveindex.info. A webpage which offers data for the refractive indices for different materials at different wavelengths.

[37] Greg Taft et al. Measurement of 10-fs Laser Pulses. *IEEE Journal of topics in quantum electronics*, 2(3):575–585, Sep 1996.

[38] Jean-Claude M. Diels, Joel J. Fontaine, Ian C. McMichael, and Francesco Simoni. Control and measurement of ultrashort pulse shapes (in amplitude and phase) with femtosecond accuracy. *Appl. Opt.*, 24(9):1270–1282, 1985.